Sustainable Cities and Society 87 (2022) 104166

Contents lists available at ScienceDirect

Sustainable Cities and Society

journal homepage: www.elsevier.com/locate/scs

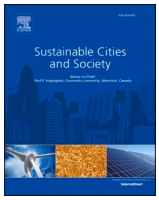

Modeling the Surface Urban Heat Island (SUHI) to study of its relationship with variations in the thermal field and with the indices of land use in the metropolitan area of Granada (Spain)

David Hidalgo-García *, Julián Arco-Díaz

University of Granada, Spain, Technical Superior School of Building Engineering, University of Granada, Fuentenueva Campus, Granada 18071, Spain

ARTICLE INFO

Keywords:
Land Surface Temperature (LST)
Surface Urban Heat Island (SUHI)
Landsat
Urban Hotspots (UHS)
Urban Thermal Field Variance Index (UTFVI)
and land use indices

ABSTRACT

Understanding just how the increase in the Earth's Surface Temperature (LST) is related to alterations of the urban climate —Surface Urban Heat Island (SUHI) or Urban Hotspots (UHS)— and with the deterioration of cities' environmental quality has become a great challenge. Societies worldwide seek actions that might break these trends and improve the quality of life of local inhabitants. In this research, with the help of Landsat 5, 7 and 8 satellite images, the evolution of land use/cover (LULC), LST and SUHI were studied over a long period, from 1985 to 2020, in the metropolitan area of the city of Granada (Spain). The aim was to evaluate how these variables, together with the Urban Index (UI), Normalized Difference Built-up Index (NDBI), Normalized Difference Vegetation Index (NDVI) and Proportion of Vegetation (PV), have influenced the variability of the UHS and the level of thermal comfort according to the Urban Thermal Field Variance Index (UTFVI). Reported as results, corroborated by statistical analysis, are mean increases in LST (2.2°C), SUHI (0.6°C), UHS (20.4%), and class 6 of the UTFV (26.2%). NDBI and UI are associated with high variations in LULCs. These have suffered increases in built-up and bare soil coverage, and decreases in water bodies, vegetation and farmland coverage.

1. Introduction

In recent years, extreme weather events tied to climate change have been acknowledged as a most urgent challenge facing society (Kovats et al., 2005; Song et al., 2020). One process contributing highly to climate change is soil modification through the expansion of urbanized areas owing to population growth (Li et al., 2011). Currently, according to a report by the United Nations, 50% of the world's population is urban; and it is expected to increase to 70% by 2050 (UN, 2018). Thus, in the next 30 years, an increase of 2,500 million inhabitants (Mukherjee & Singh, 2020) will mean growth of impervious surfaces for coverage amounting to approximately 1,527,000 km^2 (Schneider et al., 2010).

It is known that urban development is the main driver of economic and urban growth, implying an expansion of industry and transport, but it alters the urban microclimate through an increase in the Earth's mean surface temperature (LST) (Scolozzi & Geneletti, 2012; Song et al., 2020). Recent investigations have reported a positive correlation between LST and urban areas, and a negative correlation between LST and green areas: urban areas have higher temperatures than rural ones, though urban green areas have somewhat lower temperatures (Hua et al., 2020; Karakuş, 2019; Tsou et al., 2017; Yang et al., 2020). The greatest increases in temperature are mainly due to the phenomenon called Urban Heat Island (UHI), which produces a modification whose intensity is heightened by human activities (Santamouris, 2020). The authors Yao et al., 2021 found, in the cities of mainland China, that human activities were behind an increase in temperatures positively correlated with the impervious areas of urban and rural areas. Recent studies indicate that the average annual temperature of a city having more than one million inhabitants is between 1°C and 3°C higher than the surrounding non-urban areas (Khamchiangta & Dhakal, 2019).

Further studies have confirmed that the UHI generates a series of climatic, environmental and socioeconomic problems that affect the quality of life of people living in cities (Dwivedi & Mohan, 2018; Macintyre et al., 2018; Rozos et al., 2013). They include a reduction of biodiversity (Čeplová et al., 2017), the degradation of water and air quality (Feizizadeh & Blaschke, 2013), changes in the energy balance (Arnfield, 2003), an increased cost of energy (Santamouris, 2020), detrimental effects on the regional climate (Sarrat et al., 2006) and even increased mortality (Arbuthnott & Hahat, 2017).

Therefore, changes in urban land cover cause changes in the

* Corresponding author.
E-mail address: dhidalgo@ugr.es (D. Hidalgo-García).

https://doi.org/10.1016/j.scs.2022.104166
Received 13 March 2022; Received in revised form 12 May 2022; Accepted 3 September 2022
Available online 5 September 2022

microclimate, which in turn affect the physical and mental well-being of the inhabitants of urban areas (Das & Das, 2020). Spain is one of the European countries showing the greatest development of artificial coverage or built-up area. It is therefore necessary to ascertain the consequences of high temperatures in order to improve the quality of life for Spanish citizens, and report results that may be extrapolated to other geographic realms. To this end, several comfort indices can be used: the Urban Heat Island Intensity Index (UHIII), the Physiological Equivalent Temperature (PET), or the Urban Thermal Field Variance Index (UTFVI). The latter is commonly used by the scientific community to assess the thermal quality of urban areas. It allows for the identification of high-temperature spaces denoted Urban Hot Spots (UHS) (Amindin et al., 2021; Das & Das, 2020; Sharma et al., 2021) and their association with different Land Uses/Land Covers (LULC). Recent research has concluded that UHS are found within urban areas having higher UHI intensities and which correspond to areas of higher LST. These studies warn of significant increases in the LST of urban areas during the past decade, directly linked to an increase in UHS (Amindin et al., 2021; Luo & Wu, 2021; Sharma et al., 2021). A study on the industrial development authority of New Okhla (India) between the years 2011 and 2019 reports respective LST and UHS increases of 6.4°C and 33.56% (Sharma et al., 2021); a study on the city of Ahvaz (Iran) between 1995 and 2018 likewise reported increases in LST and UHS of 3°C and 4%, respectively (Amindin et al., 2021); a study involving five districts of the Suez Governorate area (Egypt) between 1988 and 2014 reported increases of 4.5°C in the LST and 16% in the areas classified as UHS (Ahmed, 2018), a study of 397 cities in China (Yao et al., 2019) reported a significant annual increase in daytime and night-time SUHI between 2001 and 2017, while one of 14 cities also in China from 1961 to 2014 (Li et al., 2021) detected a decrease in environmental humidity related to the increase in SUHI. These reported increases in LST and UHI, in view of further study results (Kafy et al., 2021; Singh et al., 2017; Vimayak et al., 2022), point to significant increases in the UTFVI classes with greater environmental discomfort for the coming years. Although the data obtained in these studies reflect some small variations in LST and UHS worldwide, they coincide in identifying industrial areas and bare soils without vegetation as the places where the largest increases are located, meaning the worst environmental quality indices.

To determine such phenomena, remote sensing stands out among the different methodologies available. It allows for large-scale urban studies of LST, UHI, UTFVI and LULC (Song et al., 2018) by means of satellite images with infrared sensors (TIRS). To understand the effects that variations in the coverage of urban areas can have on the LST and the SUHI, it is essential to analyze land use and cover (Tepanosyan et al., 2021). The evolution of these phenomena in the urban environment must be studied for mitigation purposes, to maintain some balance within a city. The information provided by research studies can equip urban areas in an effort to be more sustainable and resilient to rising temperatures caused by climate change.

The objective of this research is to study the evolution undergone by the LULC, LST and SUHI in the metropolitan area of Granada (Spain) between 1985 and 2020, in order to evaluate how these variables —together with the Urban Index (UI), Proportion of Vegetation (PV), Normalized Difference Built-up Index (NDBI) and Normalized Difference Vegetation Index (NDVI) — have influenced the variability of UHS and UTFVI. Based on Landsat 5, 7 and 8 images, NDBI, NDVI, UI, PV index maps and LULC maps were generated, using the support vector machine (SVM) method. In turn, the LST was recorded, the SUHI was obtained, the evolution of the UHS was explored, and the level of thermal comfort of the city was evaluated through the UTFVI system. Finally, statistical analysis served to determine correlations between the data obtained and the variables of study, by means of the Data Panel technique. Compared to traditional correlation methods, this approach is novel in that it admits the inclusion of individual effects of a certain area to arrive at global results. This aspect is usually overlooked by more commonly used methods, yet it provides for more complete results.

Several issues of great importance serve to justify our research: 1) The analyzed city does not have SUHI studies that contemplate a wide temporal variability like the range contemplated here. There is only one study of the spatial and temporal variability of the SUHI during a time interval of one year (Hidalgo & Arco, 2021). 2) The study period covered by this research is a positive element, allowing a view of how the indices and factors investigated vary in an extended time interval. Recent studies (Barbieri et al., 2018; Feizizadeh & Blaschke, 2013; Mukherjee & Singh, 2020) tend to use specific values of indices that are extrapolated to long periods to derive global results. Such a premise might be erroneous; recent research (Anjos et al., 2020; Emmanuel & Krüger, 2012) warns of high variability regarding the LST and UHI both over time and throughout a single day. 3) The more commonly used system for obtaining the LST, by means of in situ measurements with high-precision radiometers, is very expensive and requires significant measurement times. Contrariwise, the use of satellite images presents a significant cost reduction, as they are freely accessible on the platforms of the US National Aeronautics and Space Administration (NASA) and the European Space Agency (ESA). This methodology therefore enables one to reduce work time, given that the platforms offer images of any part of the earth since the date of the satellite launch.

The research questions that we intend to answer are the following: 1. How have the LST and SUHI variables, and the LULC, NDVI, NDBI, UI and PV indices, evolved in the area studied during the period 1985-2020? 2. What relationships exist between/among these variables? 3. How have the UHS in the study area evolved and what relationship do they have with the different LULC coverages? 4. How have the different areas of the UTFVI system evolved? 5. Could the results obtained prove important for future urban planning?

The advance that this research represents is to provide a comprehensive study on the evolution of the indices and factors indicated during the last 35 years in area of study. A better understanding of their evolution within the analyzed time interval will, hopefully, aid public administrations and urban planners at the time of decision-making, to adopt measures that mitigate the effects of phenomena that alter the urban climate, such as the Heat Island Urban (UHI). Effective and efficient measures are needed for new urban development, promoting resiliency to climate change, improved quality of life for inhabitants, and lesser harmful effects in terms of LST and UHI increases. The methodology applied, under an open source work environment, moreover allows for extrapolation of our results to other areas. We therefore uphold it as a model to be followed in future studies.

2. Materials and methods

2.1. Study area

The area studied belongs to the "plan for urban agglomeration" of the city of Granada (Andalucía), in southern Spain. Along with the city itself, this area embraces 31 smaller municipalities: Albolote, Alfacar, Alhendín, Armilla, Atarfe, Cajar, Cenes de la Vega, Cijuela, Cullar Vega, Chauchina, Churriana de la Vega, Dilar, Fuente Vaqueros, Gojar, Guevejar, Huetor Vega, Jun, Lachar, Maracena, Monachil, Ogíjares, Otura, Peligros, Pinos Genil, Pinos Puente, Pulianas, Santa Fe, Viznar, La Zubia, Las Gabias and Vegas del Genil.

The UTM geographic coordinates of the center of the area are: latitude 37.111741 N and longitude 03.362401 W; the average altitude is 680 meters above sea level (Fig. 1). The area includes the city of Granada (280,000 inhabitants) and the aforementioned small to medium-sized municipalities. In 1985 it had a population of 210,000 inhabitants and an urban area of 12,145 hectares (Ha), increasing by 2021 to 450,000 inhabitants and 37,790 Ha (Statistics National Institute (SNI) 2021). These data mark a growth of 240,000 persons and 25,645 hectares in an interval of 35 years. The local climate is conditioned by its proximity to the coast and its location along the foothills of Sierra Nevada, with an average altitude of 2,045 meters and a maximum of 3,482 meters a.s.l,

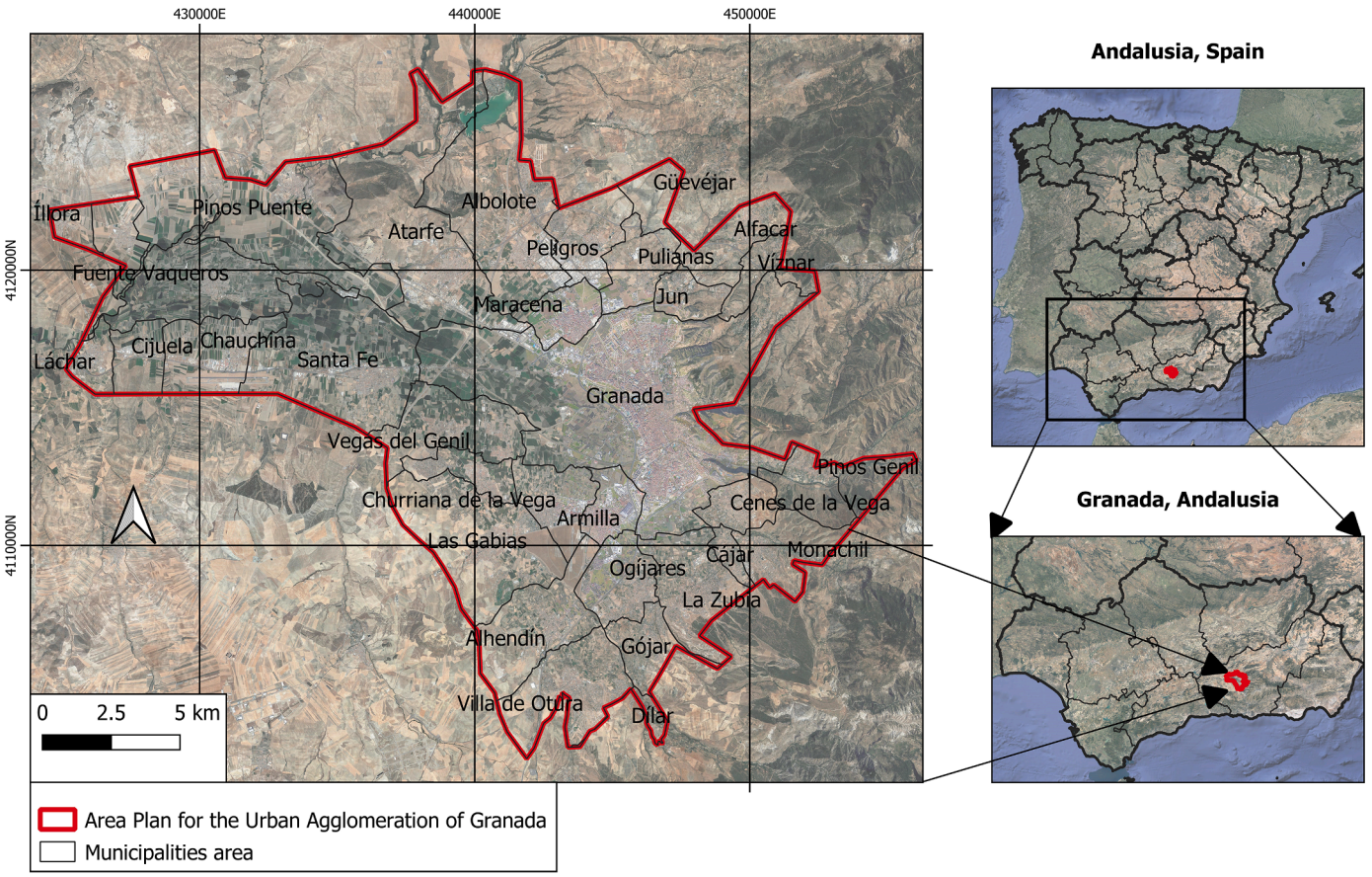

Fig. 1. Granada study area, Andalusia, Spain.

making it the second highest mountain massif in all of Western Europe, after the Alps. According to the Köppen-Geiger climate classification, the area under study has a transition climate between the cold semi-arid climate (Bsk) and the Mediterranean climate (Csa) owing to its proximity to a vast mountain system. The Csa climate features hot, dry summers and rainy winters. The Bsk climate, in turn, is considered transitional between the Mediterranean climate and the desert climate. It presents warmer temperatures overall, with dry summers and relatively dry winters (de Castro et al., 2007). The approximate number of hours of sunshine per year is 2,917, hence an average of 7.99 hours of sunshine per day. The average annual temperature fluctuates between 30.5°C in July and 6.5°C in January; there are summer extremes of 44°C and winter minima of -3°C (MSA, 2021).

2.2. Methodology

The methodology carried out for the development of this research work is shown in Fig. 2.

The NDVI, NDBI, PV, UI and LST indices were determined using Landsat 5, 7 and 8 with the open-source software QGIS, version 3.10.5. LULC maps for those years were created from the indicated images by means of the support vector machine (SVM) method. The determination of land cover relied on a precision matrix to ensure accuracy; the area to be assessed underwent cross-tabulation between the reference category and the classified one (Campbell, 1996). Its use in studies that require the classification of the land surface is well documented (Xu et al., 2009; Yoo et al., 2019). Next, the SUHI was determined, and the UHS and UTFVI of the area under study were identified with the Raster calculator tool of the indicated software. The specialized software for data science, STATA, version 16, was used for statistical analysis of the data obtained in our study.

2.3. Landsat data

Landsat 5, 7 and 8 images were obtained from the United States Geological Survey (USGS) for the years indicated below:

- Landsat 5 (Bands 2 to 6): Years 1985, 1990 and 1995.
- Landsat 7 (Bands 2 to 6): Years 2000, 2005 and 2010.
- Landsat 8 (Bands 2 to 6 and 10): Years 2015 and 2020.

The Landsat data set with their optical bands were used to determine the indices: NDVI, NDBI, LULC, PV and UI; the thermal band was used to retrieve the LST values.

Landsat 5 Thermal Mapper (TM) data cover a total of one thermal infrared band (band 6) with a resolution of 120 m and six multispectral bands (bands 1 to 5 and 7) with a spatial resolution of 30 m. Landsat 7 has six multispectral bands (bands 1 to 5 and 7) with a spatial resolution of 30 m, plus one thermal band (band 6) on the Enhanced Thermal Mapper Plus (ETM+) sensor with a spatial resolution of 60 meters. Finally, the two Landsat 8 scanning instruments —Operational Land Sensor/Thermal Infrared Sensor (OLI/TIRS)— have a total of two thermal infrared bands (bands 10 and 11) with a spatial resolution of 100 m, and 8 multispectral bands (bands 1 to 7 and 9) with a resolution of 30 m. Yet for the determination of the LST with Landsat 8, only band 10 was used. The Landsat 5 bands were resampled at a spatial resolution of 30 meters, while the Landsat 7 and 8 bands were resampled at a resolution of 15 meters thanks to the use of a panchromatic band.

The area of study is located under the path of the Landsat 5, 7 and 8 satellites. The data set was acquired for the month of April of each year, when the weather in Spain is usually sunny and mild, therefore allowing for better discrimination of the different land uses. Throughout this time interval, 24 images were used (three per year, 1985: 07, 15 and 24;

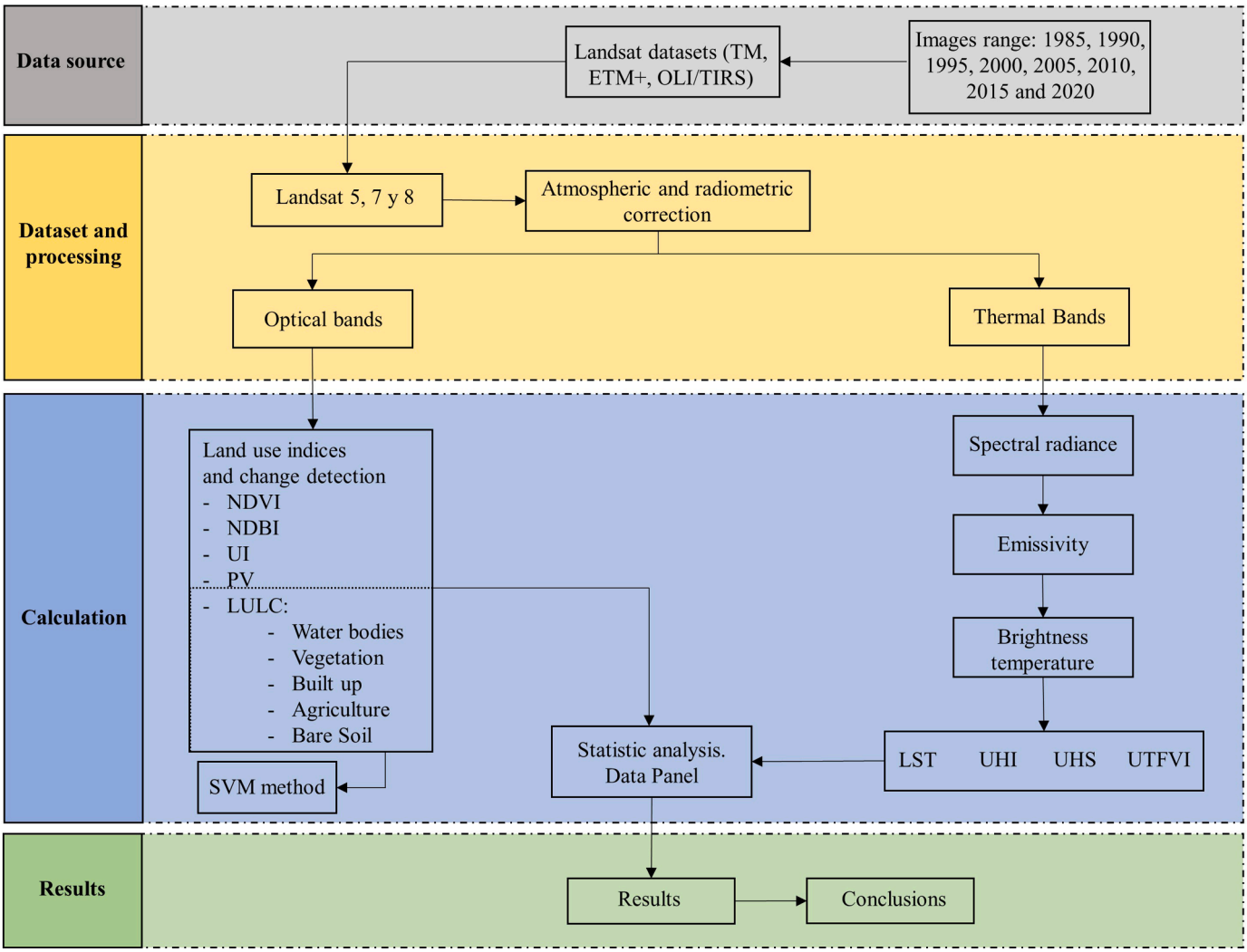

Fig. 2. Methodology.

1990: 06, 13 and 22; 1995: 04, 11 and 20; 2000: 01, 13 and 24; 2005: 06, 15 and 22; 2010: 02, 14 and 26; 2015: 02, 16 and 23; and 2020: 04, 11 and 20), having a cloudiness index of less than 15 to enhance accuracy in obtaining the LST and subsequent SUHI. The selected images were georeferenced using the ETRS89/UTM Zone 30N projection system. Atmospheric correction in OLI bands relied on the DOS (Dark Object Subtraction) algorithm (Chavez, 1988; Li & Meng, 2018; Zhang et al., 2015) and the Semi-Automatic Classification Plugin (SCP) with the open-source software environment QGIS, version 3.10.5 (Congedo, 2016; Rozenstein et al., 2014).

2.4. Thermal bands

2.4.1. Spectral radiance (L_λ)

To obtain the spectral radiance from the digital numbers (DN) of the TIRS band, the following equation was used (Kafer et al., 2019):

$$L_\lambda = M_L \times Q_{Cal} + A_L, \quad (1)$$

where L_λ is the spectral radiance of the upper part of the atmosphere (TOA) expressed in W/(m^2•sr•μm); M_L is the specific multiplicative factor of the band that is located in the metadata file of the Landsat images. For TIRS bands this factor is 3.342 × 10^{-4} W/ (m^2•sr• μm); Q_{Cal} is the digital value (DN) of the bands that ranges from 0 to 255; and A_L is the additive rescaling factor specific to the TIRS bands, also included in the image metadata files.

2.4.2. Brightness temperature

Spectral radiation (TOA) was converted to brightness temperature (T) in°C using equation 2. The thermal conversion constants K1 and K2 of the TIRS bands attached in the data file served to this end. The formula used is as follows (Kafer et al., 2019; Weng et al., 2004):

$$T = \frac{K_2}{\log\left(\frac{K_1}{L_\lambda} + 1\right)} - 273.15, \quad (2)$$

where L_λ is the spectral radiance derived from equation 1, and K_1 and K_2 are the thermal conversion constants of the TIRS bands that appear in the metadata files (Landsat 5: K_1= 607.76 and K_2= 1260.56; Landsat 7: K_1= 666.09 and K_2= 1282.71; Landsat 8: K_1= 774.8853 and K_2= 1321.0789).

2.4.3. Land surface emissivity (ε)

The earth's surface and its various components have different emissivities. This factor was determined by applying equation 3 based on the NDVI: (Sharma et al., 2021):

$$\varepsilon = 0.004 \times \mathrm{Pv} + 0.986, \quad (3)$$

where Pv is the proportion of vegetation derived from the NDVI (equation 7).

2.4.4. Land surface temperature (LST)

In view of the emissivity values of the earth's surface (LSE), the Land Surface Temperature (LST) was determined by means of equation 4 (Weng et al., 2004):

$$LST = \frac{T}{\left(1 + \left(\lambda \ \frac{T}{C_2}\right) x \log(\varepsilon)\right)} \tag{4}$$

$$C_2 = \frac{h \ x \ c}{s}, \tag{5}$$

where LST is the land surface temperature, λ is the wavelength of the emitted radiation (Landsat 5 and 7: λ =11.457 μm and Landsat 8: λ =10.8 μm), T is the Landsat brightness temperature, ε is the emissivity of the ground, $C_2 = 1.4388 \times 10^{-2}$ m K, h is Planck's constant with a value of 6.626×10^{-34} Js, s is the Boltzmann constant with value 1.38×10^{-23} J/K, and c is the speed of light with a value of 2.998×10^{8} m/s (Weng et al., 2004).

2.5. Optical bands

2.5.1. Land use/Land cover (LULC)

LULC maps were prepared from Landsat images by composing a red, green, and blue (RGB) band plan. Next, using the support machine method (SVM) and the QGIS software, the LULC plans were derived. This methodology has been used in numerous investigations (Otukei & Blaschke, 2010; Shafri & Ramle, 2009) to distinguish land use with high precision (Amindin et al., 2021). In our research, five main land uses were identified: water bodies, vegetation, built-up, agriculture, and bare soil.

2.5.2. NDVI calculation threshold method ($NDVI^{THM}$)

The normalized vegetation index (NDVI) is calculated using the optical bands of the near infrared (NIR) and the red band (Red). This index allows us to estimate the presence of vegetation in an area. The range of NDVI values is between -1 and 1. The first indicates clear and sparse soils, while the second indicates dense vegetation. It is calculated using the following formula:

$$NDVI = \frac{NIR - Red}{NIR + Red} \tag{6}$$

With the values determined in equation 6, the proportion of vegetation (PV) can be calculated. This index determines the proportion of an area that is covered by vegetation or another type of soil (Rajeshwari A, 2014). Equation 7 for the calculation of the PV is derived from the NDVI (Yu et al., 2014):

$$PV = \left[\frac{NDVI - NDVI_{min}}{NDVI_{max} - NDVI_{min}}\right]^2, \tag{7}$$

where NDVI is the normalized vegetation index calculated using formula (6) and $NDVI_{max}$ and $NDVI_{min}$ are the maximum and minimum NDVI values of the interval.

2.5.3. Normalized difference built-up index (NDBI)

To calculate the NDBI, the short wave infrared (SWIR) and NIR bands were used according to equation 8 (Zha et al., 2003):

$$NDBI = \frac{NIR - SWIR}{NIR + SWIR} \tag{8}$$

2.5.4. Urban index (UI)

The UI was calculated using $SWIR_2$ and NIR bands following equation 9 (Kawamura et al., 1996):

$$UI = \frac{SWIR_2 - NIR}{SWIR_2 + NIR} \tag{9}$$

2.6. Surface urban heat island estimation

According to the existing literature on the determination of the SUHI, it is obtained by means of the temperature difference between the measurements made simultaneously in the urban area and the rural area (Oke, 1987). Therefore, the SUHI can be determined according to equation 10:

$$SUHI = TST_{urban} - TST_{rural} \tag{10}$$

The urban LST values correspond to the average values of the pixels located within the urban area. The rural area chosen to derive the SUHI through the temperature differences from the urban area corresponds to where the Spanish State Meteorological Agency (AEMET) has a rural weather station. It lies 16 km outside the city, and there are no paved areas within a radius of 1000 m. Using the raster calculator command of the QGIS software and the exported Landsat images, the SUHI of Granada was determined by equation 10.

2.7. Urban Hotspots (UHS)

Hot spots are identified based on the LST within the study area. They are zones of variable size found within places showing the highest temperatures, and they are usually considered as uncomfortable for human activities. These spaces are determined using the following formula (Guha, 2017; Jafari et al., 2021; Sharma et al., 2021):

$$LST > \mu + 2 * \sigma, \tag{11}$$

where μ and σ are respectively the mean value and the standard deviation of the LST of the zone in °C. Using this equation the areas that present urban zones with LST values above the mean and with a confidence interval greater than 95% can be determined.

2.8. Urban thermal field variance index (UTFVI)

This index allows the value of each pixel of the urban area to be appraised in relation to the entire area, so as to obtain a classification of environmental quality (Sobrino & Irakulis, 2020; Vimayak et al., 2022). The UTFVI values fall into six typologies, in turn presenting six classes of ecological evaluation (Table 6). Each is related to the degree of presence of the SUHI phenomenon and its impact on the environmental quality of the population (Liu & Zhang, 2011). The UTFVI classes, based on the strength of the SUHI, range from 1 (excellent) to class 6 (worst), determined using the following equation (Guha et al., 2018; Vimayak et al., 2022):

$$UTFVI = \frac{LST - T_{mean}}{T_{mean}}, \tag{12}$$

Here, LST is the temperature of each pixel (°C) and T_{mean} is the average LST of the entire area (°C). UTFVI values below zero indicate the complete absence of the UHI phenomenon, meaning it is a site where maximum thermal comfort occurs, hence an area classified as having excellent environmental quality. As UTFVI values increase, SUHI intensity also increases, and therefore thermal comfort deteriorates (Sharma et al., 2021).

2.9. Strategy of analysis

Panel data refers to a statistical analysis that combines a temporal dimension (time) with a cross-sectional dimension (data or values). This method is often cited in the literature and involves the use of multiple regression models (Alcock et al., 2015; Chen et al., 2011; Fang & Tian, 2020), which allows for a larger amount of data to be included than under traditional methods. There are three calculation options: ordinary squares method (OSM), generalized least squares (GLS), and intragroup estimation method (IEM) (Labra, 2014). To ascertain which of these

three should be applied, the following steps must be carried out (Chen et al., 2011). 1) Using the Hausman test, determine if the effects of the analysis are fixed or random; this allows the method to determine different hypotheses about the behaviour of the residuals of statistical analysis. 2) Evaluation of the model using the Wooldridge and Wald tests. Both stages will indicate the most appropriate method to use (Seto & Kaufmann, 2003). Our statistical analysis was performed with STATA software, version 16. After carrying out the indicated tests, the IEM method with random effects was used according to equation 2:

$$Y_{it} = \beta X_{it} + (\alpha_i + \mu_{it}), \quad (13)$$

where μ_{it} is the error of the model, α_i represents the individual effects, X_{it} are explanatory variables, β is an independent variable, t=time and i=individual.

3. Results

3.1. Space-time evaluation of spectral indices (LULC, NDVI, NDBI, PV and UI)

The measures of central tendency and dispersion of the spectral indices NDVI, NDBI, PV and UI between the years 1985 and 2020 can be found in Fig. 3, while the space-time analysis of the spectral indices is represented in Figs. 4, 5 and 6.

The NDVI index presents the highest mean value, 0.368, in the year 2015, whereas the lowest mean value is 0.225 in the year 2005. The PV index gives the highest mean value of 0.627 in the year 1995, the lowest mean value being 0.179 in 1985. These values report average reductions of -3.41% and -28.09%, respectively, over the study period. The mean values of the NDVI and PV indices decreased, respectively, from 0.323 to 0.312 and from 0.445 to 0.320. Given that the selected images correspond to springtime, the vegetation of the studied area can be considered as scattered. The values are more intense in the zone toward the southeast of the study area, corresponding to the rural zone having vegetation or cultivation. The less intense values coincide with the city of Granada and its neighbouring municipalities.

The NDBI index presents the highest mean value of 0.095 in the year 2010; the lowest mean value is 0.015 in the year 1995. The UI index presents the highest mean value of 0.223 in the year 2020, while the mean value is lowest, 0.179, in 1985. These values attest to overall increases in the indices during the period under study, of 14.3% and 24.6%, respectively. The mean values of the NDBI and UI indices went from 0.077 up to 0.088 and from 0.179 to 0.223, respectively. Such findings point to excessive built-up land coverage, well in line with the increase of 3,245 hectares built-up (Table 2) in the years studied. The most intense values are seen to coincide with urban sectors within the area studied.

Figure 4 and Table 1 display our analysis of the local coverage, broken down by categories. Water bodies present their highest value (1069 ha) in the year 2005; their lowest value (166 ha) occurs in 2000. Vegetation gives its highest value, 5367 ha, in 2000, whereas the lowest value of 2600 ha occurs in the year 2010. Built-up shows the lowest value, 8100 ha, in the year 1985; the highest value is seen for 2020, with 10745 ha. Farming presents the lowest mean value of 4827 ha in the year 2020, while the highest mean value of 10175 is found for the year 1985. Lastly, bare soil coverage presents the lowest mean value of 13000 ha in the year 1985, whereas the highest mean value of 16412 ha is recorded within 2020. Such values denote significant decreases from 1985 to 2020 of soils identified as water bodies, vegetation and farming: of -48.3%, -10.8% and -52.6%, respectively. Contrariwise, increases of 40.1% and 28.7% are reported for land covers identified as built-up and bare soil, respectively. The increase in bare soil coverage might be due to an abandonment of farmland motivated by high production costs, droughts, progressive industrialization, and/or land speculation by developers —all common circumstances in the arable lands of the Mediterranean basin. Still, according to the data shown in Table 1, the latter coverages increased consistently throughout the period studied.

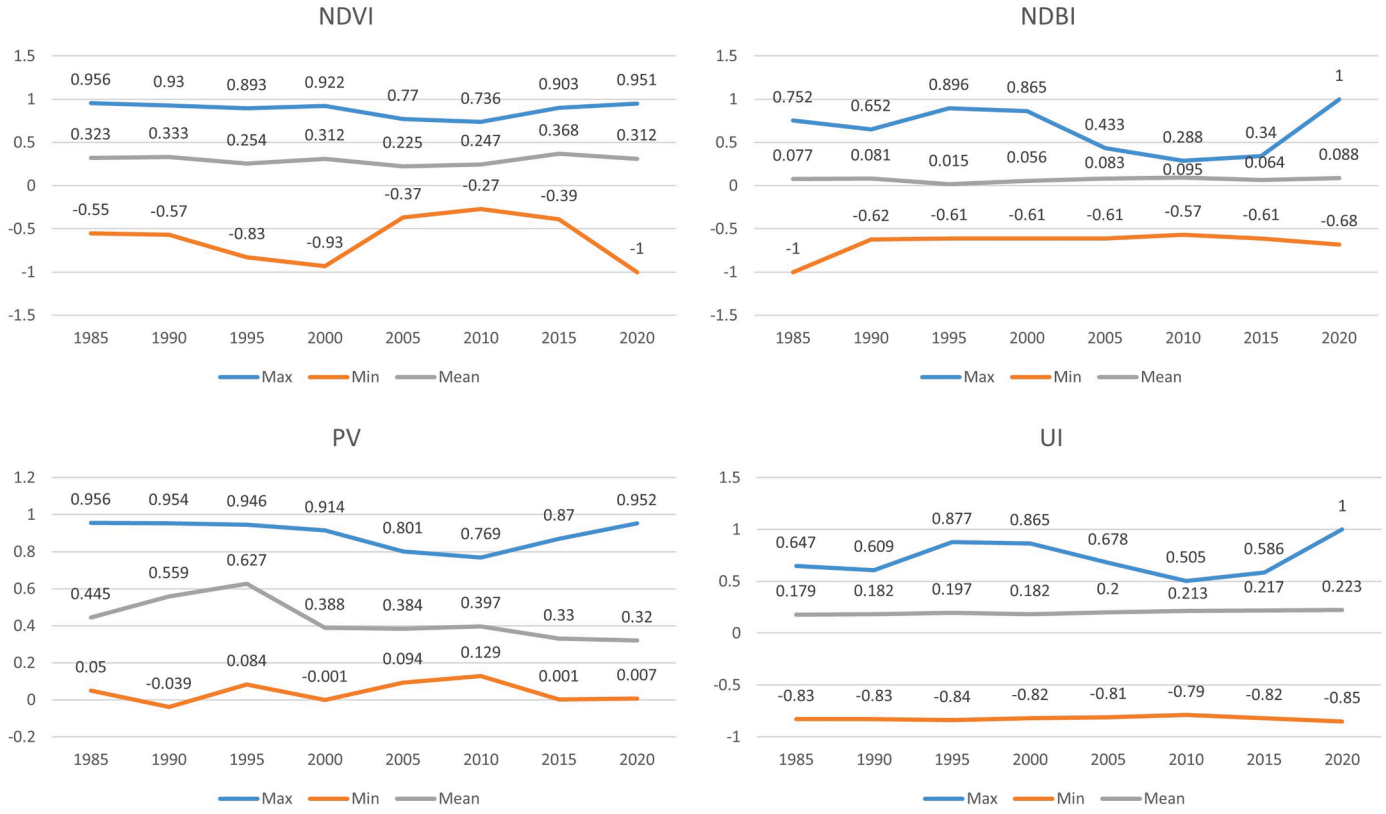

Fig. 3. Dispersion measures of NDVI, NDBI, PV and UI indices per year.

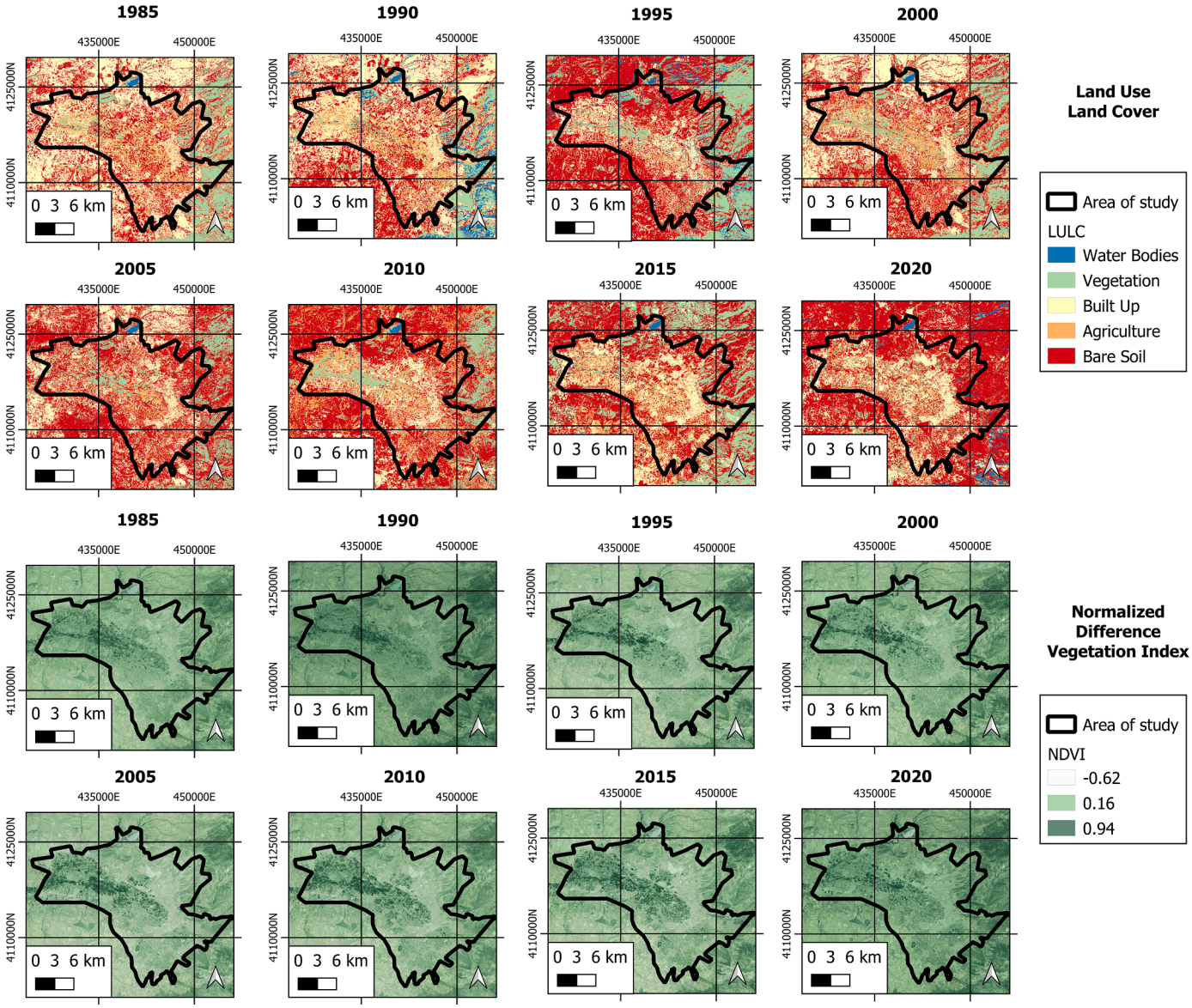

Fig. 4. Land Use Land Cover and Normalized Difference Vegetation Index by study date.

Meanwhile, the coverages of farming, vegetation and water bodies present non-constant decreases with strong oscillations. This could indicate that the development of such areas also depends on climatic conditions, which vary each year depending, particularly, on the rainfall.

The greatest changes in the LULC are found for the northern sector of the study area, which reflects a significant increase in bare soil cover. In contrast, up to the year 2010, a wide area destined for vegetation grows to the northwest, then begins to decrease in the observations in years 2015 and 2020.

Seen in Table 2 are the results of the precision matrix carried out to verify the LULC maps obtained. The precision was 83%, with a 95% confidence interval that varies between 0.77 and 0.89 points. The Tau value is 0.795; the Kappa coefficient obtained is 0.785. After determination of the matrix, however, manual correction was applied to the points that did not coincide with the LULC maps obtained.

3.2. Spatio-temporal evaluation of LST and SUHI

Figures 7 and 8 show the space-time analysis of the LST and the SUHI between 1985 and 2020 in the area studied. Table 3 presents the measures of central tendency and dispersion of both variables. In general, urban areas are seen to have high LST values as opposed to rural areas.

The lowest maximum LST value was 44.1°C in the year 1995, whereas the highest value was 51.8°C in the year 2015. The lowest minimum LST value, 17.9°C, occurred in 1990; the highest value was 26.1°C in the year 2015. As for the mean minimum LST, the lowest value was 32.6°C in the year 2000, and the highest value was 35.2°C in 2020. The spatial statistics of LST show a steady increase over the period 1985-2020 of 2.2°C, which means an increase of 6.6%. Yet the maximum and minimum values show greater increases in their trends, with respective values of 7.7°C and 8.2°C. In contrast, even though the average values also grow, they do so at a lower rate —with an increase of 2.6°C. As clearly seen in Fig. 7, the LST increases tend to take place homogeneously throughout the studied area up to 2010, when they show a strong increase. The areas with lower temperatures are found to coincide with the areas presenting higher values for NDVI and PV, and lower values for NDBI and UI indices.

Altogether, the lowest maximum SUHI value was 3.2°C in the year 2005, and the highest value was 5.2°C in 2020. The lowest minimum SUHI value was -3°C in year 1985, while the value was highest in 1990,

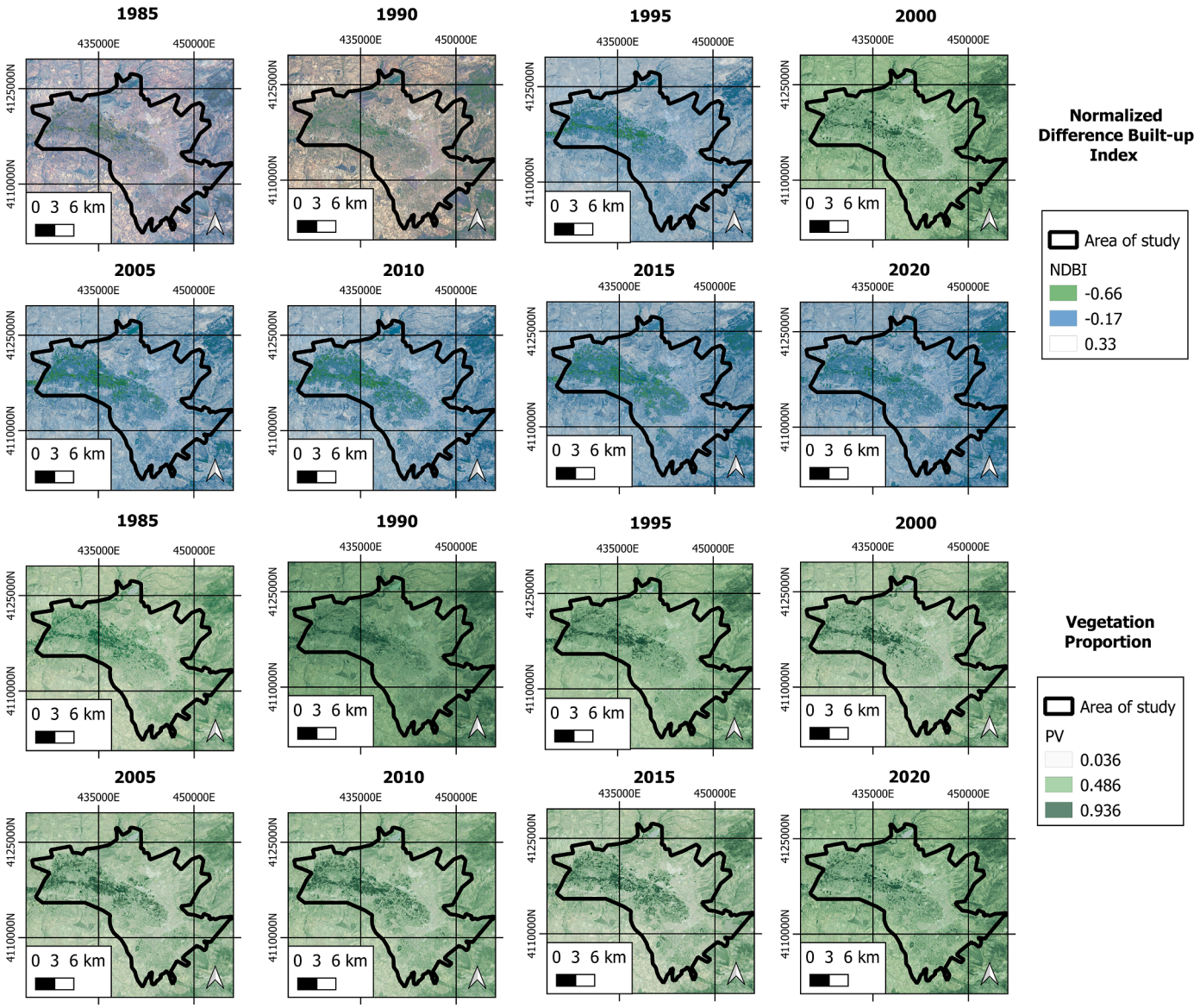

Fig. 5. Normalized Difference Built up and Vegetation Proportion indices by study date.

-4.8°C. The lowest mean minimum LST value was 0.10°C in the year 1985; the highest was 0.7°C in 2020. The spatial statistics of SUHI for the studied area show a gradual, continuous increase during the period 1985-2020 of 0.6°C, which represents an increase of 600%. Notwithstanding, and as occurs with the LST values, the maximum and minimum SUHI values show even greater increases, with values of 2.0°C and 1.3°C, respectively. The average values also grow, but they do so at a lower rate, of 0.6°C.

According to Fig. 8, the increases in SUHI also occur homogeneously throughout the study area up to the year 2010, when they mark a sharp increase. Areas with lower SUHI temperatures are seen to coincide with the areas presenting higher NDVI and PV indices, and lower values for NDBI and UI. Hence it may be stated that urban areas have higher SUHI values than rural areas.

3.3. Identification of UHS

Figure 9 offers a space-time analysis of the UHS in the area studied, 1985 to 2020. The reader can easily spot a significant increase in the area classified as UHS in the area under study —particularly visible from the 2005 readings onward.

Table 4 presents the critical values by year for determination of the UHS zones, as well as their extension and the percentage of occupation with respect to the total area studied. In general terms, over the years studied, the UHS area increased from 544 ha (1.4% of the total area) to 8,318 ha (22.0% of the total area), hence an increase in the sector classified as UHS of 7774 ha (20.6%) from 1985 to 2020. Growth is constant between the years 1985 and 2010, and significant between 2010 and 2015.

In 1985, the UHS zones (1.4%) were located to the south of Granada and coincided with the military air base in the town of Armilla, a vast area without vegetation cover. From 2010 onward new UHS areas begin to appear in a disaggregated manner in the area under study. In 2015 the UHS zones reach a significant percentage (19.5%) of extension, albeit irregular, in the entire study area.

In Fig. 10, the zones classified as UHS and the space-time variability of the SUHI between 1985 and 2020 are jointly represented. The places where the SUHI presents greater intensities are seen to coincide with the zones classified as UHS; the areas having lower intensities of SUHI are not classified as UHS.

These findings served to identify any coverage involved in presenting higher temperatures and located within areas classified as UHS.

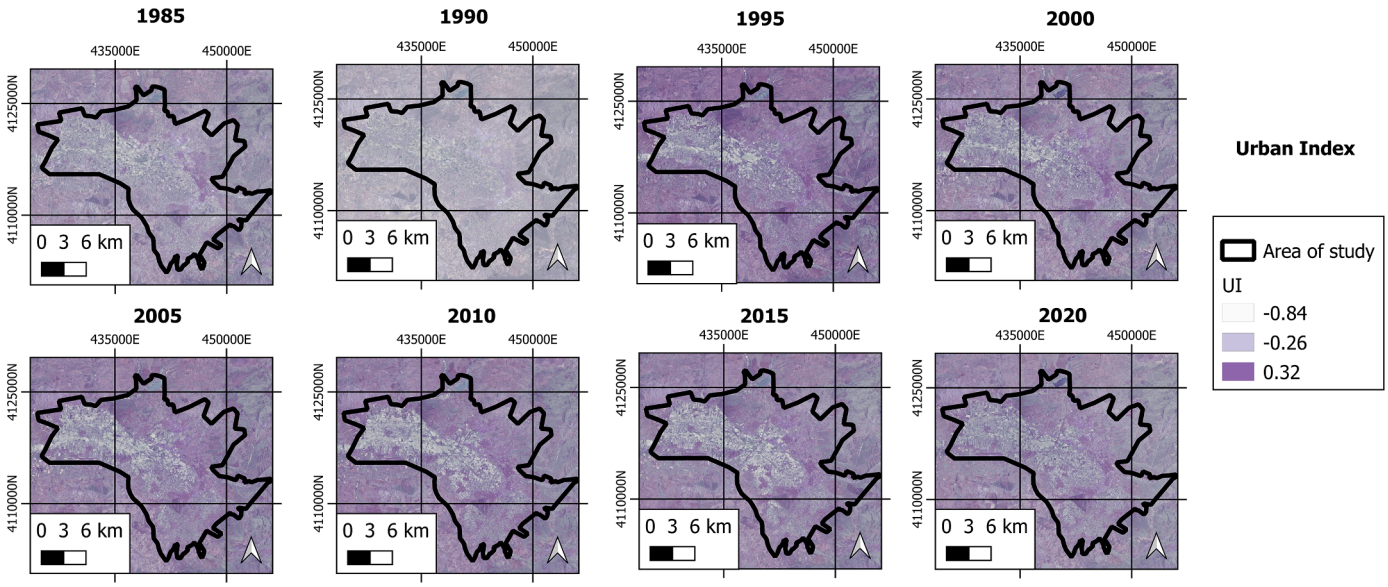

Fig. 6. Urban Index Index by study date.

Table 1
Variation in land use per year.

LULC (Ha)	1985	1990	1995	2000	2005	2010	2015	2020	Variability (%) (1985-2020)
Water bodies	677	893	1069	166	169	190	216	350	-48.3
Vegetation	3853	3670	4790	5367	4174	2600	3700	3436	-10.8
Built-up	8100	8700	9742	9869	10028	10150	10356	10745	40.1
Farming	10175	9000	6294	6731	6084	7571	5800	4827	-52.6
Bare soil	13000	13537	13900	13657	15330	15330	15703	16412	28.7

Table 2
Precision Matrix.

	1	2	3	4	5	UA (%)
1	10	0	0	0	0	100
2	0	80	0	0	0	100
3	0	0	20	0	2	10
4	0	0	5	10	0	50
5	0	0	0	0	10	100
PA (%)	100	100	75	100	24	130

Note: 1: Water bodies. 2: Vegetation. 3: Built-up. 4: Farming. 5: Bare soil. PA (5): Producer accuracy. UA (5): User accuracy.

Accordingly, the UHS would occupy a surface of 283 ha (3.4%) of the coverage called vegetation, a surface of 3311 ha (39.8%) of that built-up, a surface of 266 ha (3.2%) of the farming coverage, and 4,466 ha (53.7%) of bare soil coverage. Thus, the covers presenting the highest concentrations of UHS are: bare soil and built-up. Contrariwise, the covers that present lower concentrations of UHS are: vegetation and farming. Water body coverage is not related to any area classified as UHS.

Figure 11 illustrates the areas classified as UHS and the LULC coverage plan of the area under study for the year 2020. A focus on the coverages that present the largest UHS areas (Fig. 11) points to areas of industrial use, featuring warehouses with metallic structures and/or roofing, large buildings, sports centers, urban green areas with little vegetation, commercial areas, roads of great width, and parking areas. The areas without vegetation or with little vegetation are where the highest concentrations of UHS are located within the bare soil cover.

3.4. Evaluation using UTFVI

Figure 12 offers the space-time analysis of our UTFVI evaluation of Granada between 1985 and 2020. An important growth of the red areas (qualified as strongest) is clearly noted. They are classified as worst for urban development in terms of already high temperatures. Table 5 shows the variability of each of the UTFVI zones by year studied. In general, the area under study has two major surfaces: class 1 (excellent) and 6 (worst).

The first presents optimal thermal comfort with UTFVI values under 0, whereas the second reflects areas of high temperatures and UTFVI values over 0.02. The areas having the highest NDVI and PV indices are located precisely in the excellent thermal comfort zones, while the built-up areas and zones with high values for NDBI and UI are located in the "worst" thermal comfort zones.

Throughout the period under study, classes 1, 2 and 3 of UTFVI show land decreases of -25.5%, -17.3% and 40.5%, respectively. Meanwhile, soil classes 4, 5 and 6 present respective soil increases of 62.4%, 6.4% and 26.2%. In 2020, 48.9% (18,478 ha) of the area under study gave an ecological index UTFVI of class 6, the worst ecological indicator considered here.

3.5. Statistical analysis

3.5.1. Relationship between LST and the NDVI, NDBI, PV, UI and LULC indices

The statistical analysis, carried out using the Data Panel method, served to determine relationships between the LST and the NDVI, NDBI, PV, UI and LULC indices of the area under study. First, the Pearson correlation coefficient was determined, then the Data Panel was developed. For the latter, the Generalized Least Squares (GLS) method was applied through equation 13. Results are indicated in Tables 6 and 7.

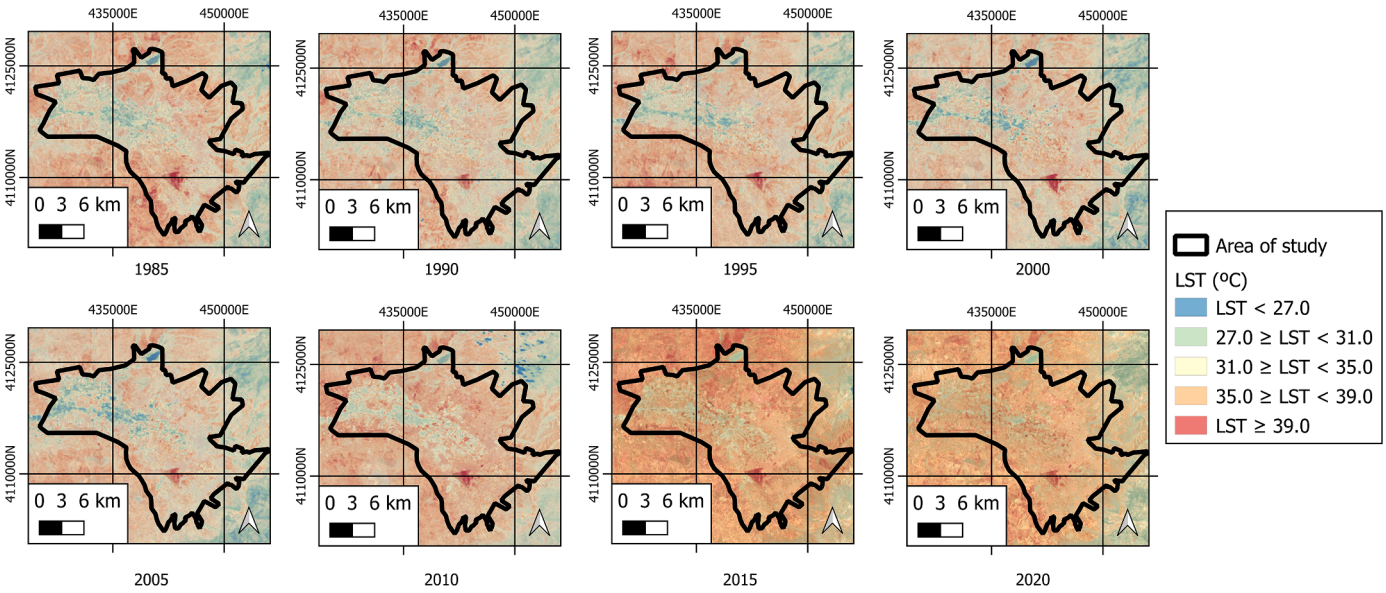

Fig. 7. Variability of the LST of the area studied by years.

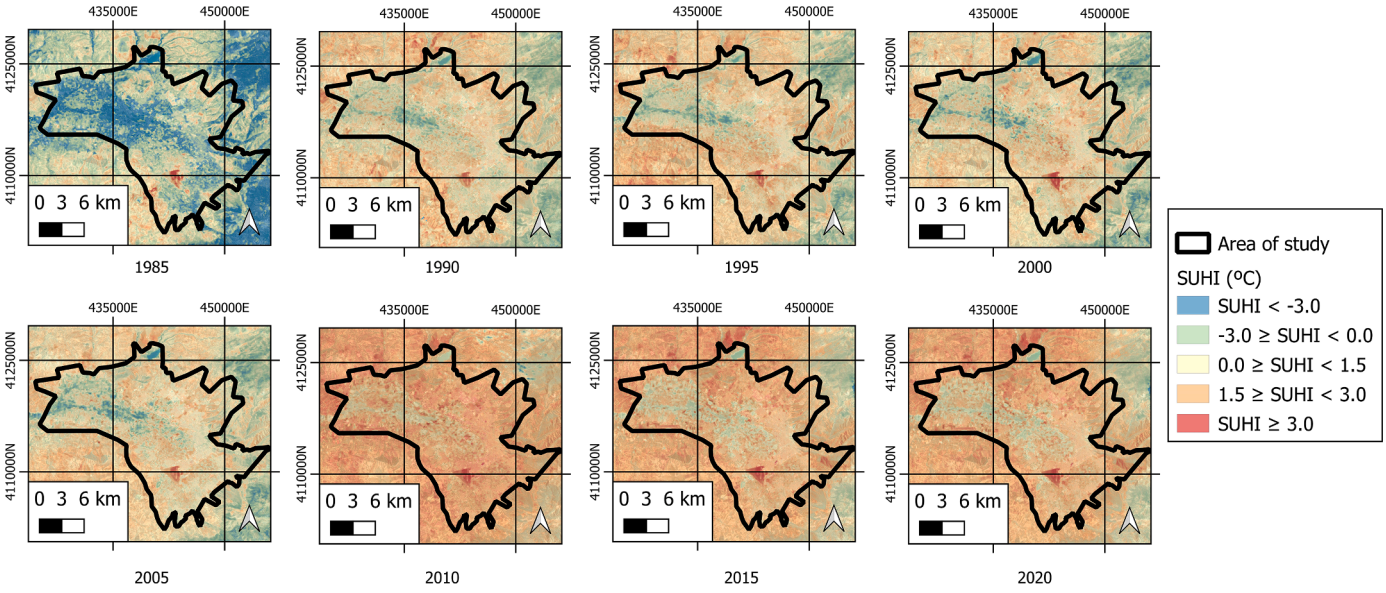

Fig. 8. SUHI variability of the studied area by years.

Table 3
Dispersion measures of LST and SUHI.

	LST (°C)				SUHI (°C)			
Year	Max	Min	Mean	SD	Max	Min	Mean	SD
1985	47.1	21.9	33.0	3.514	3.7	-3.5	0.1	1
1990	45.2	17.9	33.4	3.216	3.7	-4.8	0.2	1
1995	44.1	19.3	33.6	3.045	3.6	-4.5	0.2	1
2000	45.2	19.7	32.6	3.227	3.9	-4.0	0.3	1
2005	45.6	21.1	34.1	3.54	3.2	-3.7	0.4	1
2010	47.1	19.7	34.5	3.263	4.5	-3.9	0.6	1
2015	51.8	26.1	34.9	3.42	3.5	-4.0	0.6	1
2020	47.1	21.8	35.2	2.701	5.2	-4.2	0.7	1

Note: SD: Standard deviation.

Overall, the LST presents strong positive correlations with the NDBI (0.812), UI (0.654) and LULC (0.678) indices, as well as an inverse relationship with the NDVI (-0.789) and PV (-0.539) indices. Based on the Data Panel, results give a statistically significant and negative relationship greater than 99% between the LST variables and the NDVI and PV indices; a positive one of 99% with the NDBI and UI index; and positive above 99% with the LULC index. The values of R^2, F statistic and Prob>chi^2 obtained show good concordance between the variables, with an adjustment level over 99% significance, since Prob>chi^2=0.000.

3.5.2. *Relationship between LST and SUHI*

The results of the data analysis are indicated in Tables 8 and 9.

The LST presents a strong positive correlation with the SUHI (0.818).

According to the statistical analysis technique of the Data Panel, our results underline a statistically significant and positive relationship above 99% between the LST and SUHI variables. The values of R^2, F statistic and Prob>chi^2 obtained show good concordance between the dependent variable and the independent ones used, with an adjustment level higher than 99% significance, since Prob>chi^2=0.000.

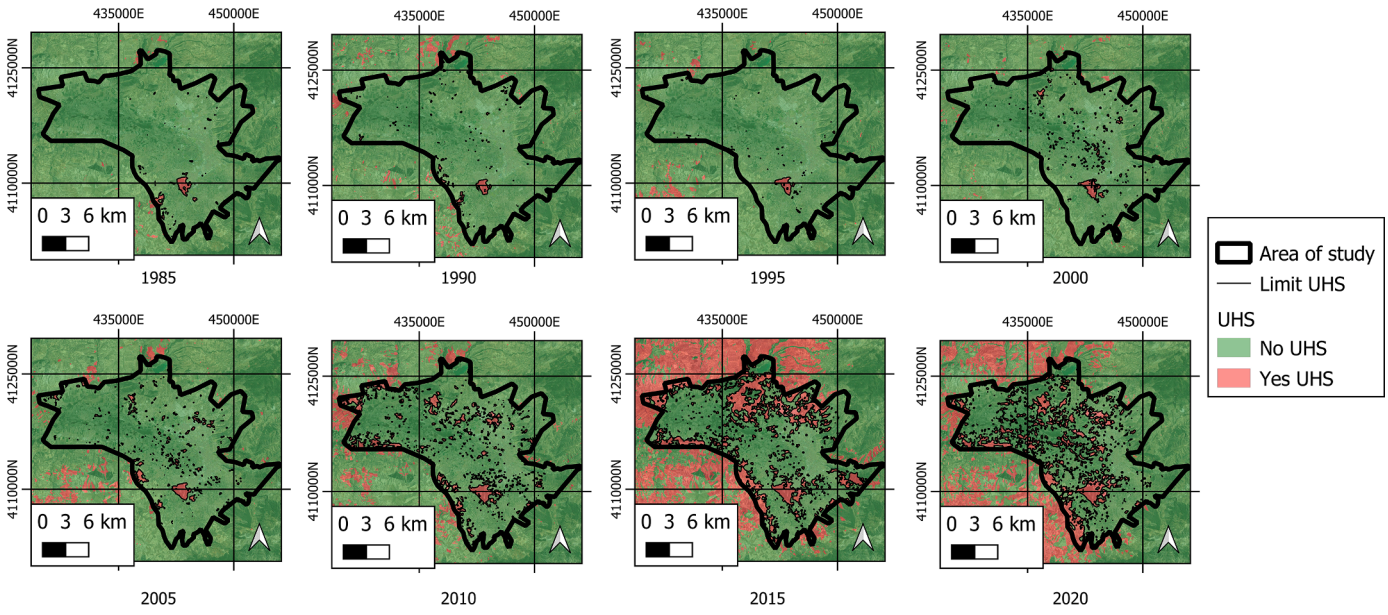

Fig. 9. UHS variability of the studied area by years.

Table 4
Average and critical LST for the determination of UHS, along with occupation.

Year	Mean LST (°C)	SD (°C)	Non UHS (°C)	UHS (°C)	UHS (ha)	UHS (%)
1985	33.0	3.514	< 40.0	> 40.0	544	1.4
1990	33.4	3.216	< 39.9	> 39.9	1523	4.0
1995	33.6	3.045	< 39.7	> 39.7	1474	3.9
2000	32.6	3.227	< 39.1	> 39.1	1568	4.2
2005	34.1	3.54	< 41.1	> 41.1	1738	4.6
2010	34.5	3.263	< 41.0	> 41.0	4421	11.7
2015	34.9	3.42	< 41.7	> 41.7	7369	19.5
2020	35.2	2.701	< 40.6	> 40.6	8318	22.0

Note: SD: Standard deviation. UHS: Urban Hot Spot.

3.5.3. *Relationship between UHS and LST, SUHI and LULC*

The results of the data analysis are indicated in Tables 10 and 11. In general, the UHS present strong positive correlations with the LST (0.859) and SUHI (0.672), plus a weak relationship with the LULC (0.195).

Data Panel results report a statistically significant and positive relationship above 99% between the variables UHS and LST and SUHI, and a positive relationship of 95% with LULC. The values of R^2, F statistic and Prob>chi^2 obtained would attest to good concordance between the dependent and independent variables used, the adjustment level being of 99% significance, with Prob>chi^2>0.000.

4. Discussion

This study explored the space-time variability of the LST, SUHI, UHS and UTFVI from 1985 to 2020 in the "urban agglomeration plan" area of the city of Granada, linking these data to the NDVI, NDBI indices, PV, UI and LULC. Our motivation stemmed from the growing number of studies indicating that changes in these indices bear a significant impact on the regional microclimate, reflected in increases in LST, SUHI and UHS.

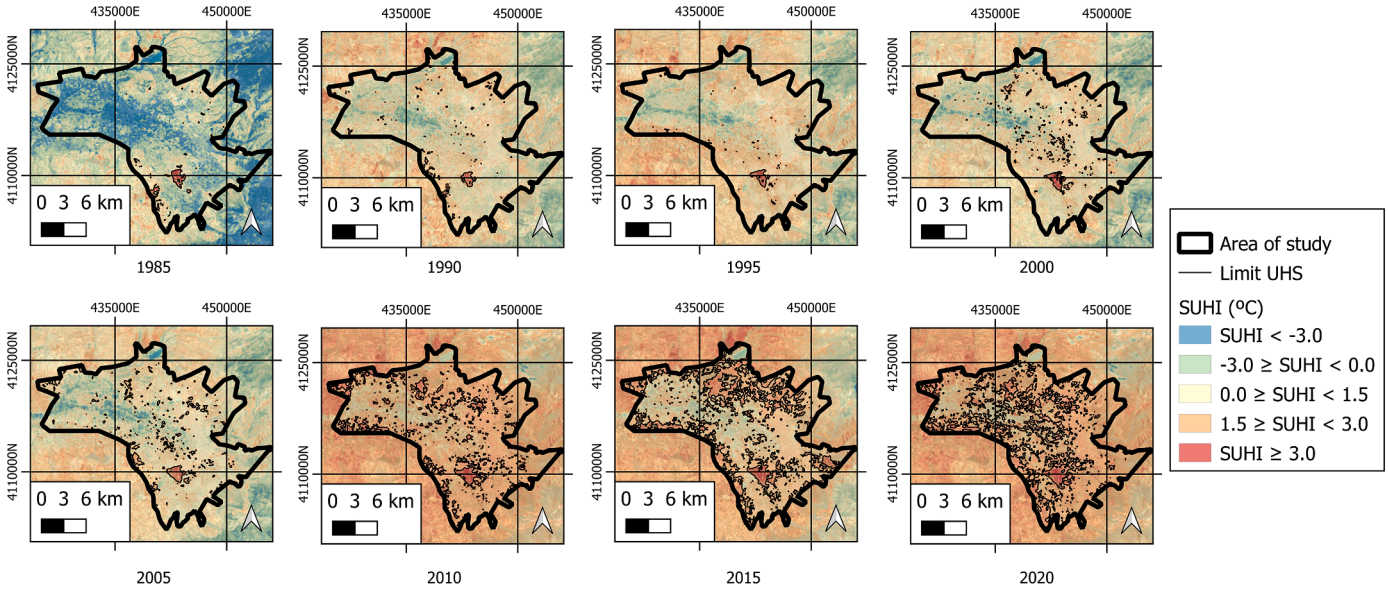

Fig. 10. Variability of SUHI and UHS of the area studied, by years.

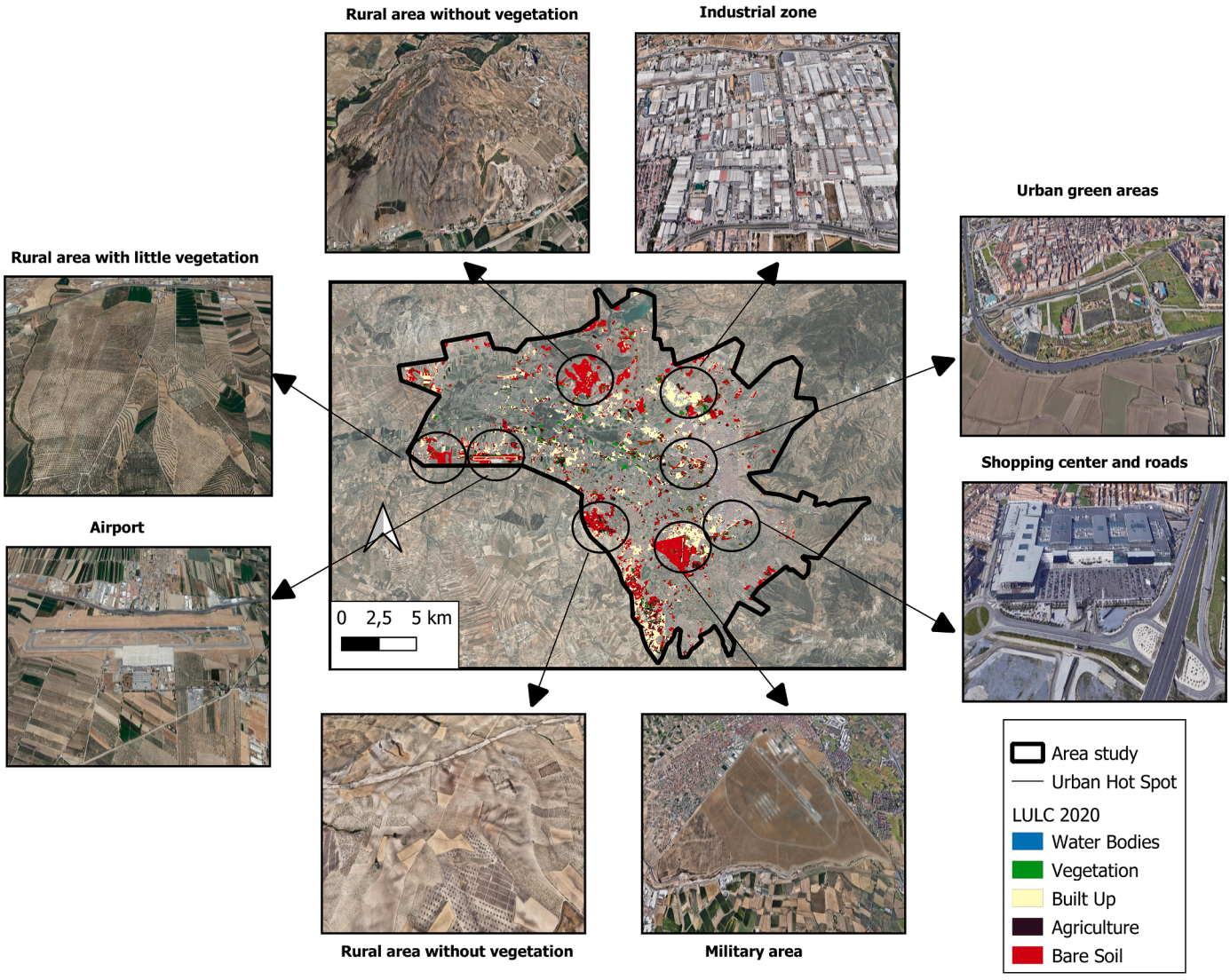

Fig. 11. Location of UHS and coverage of the area studied in 2020.

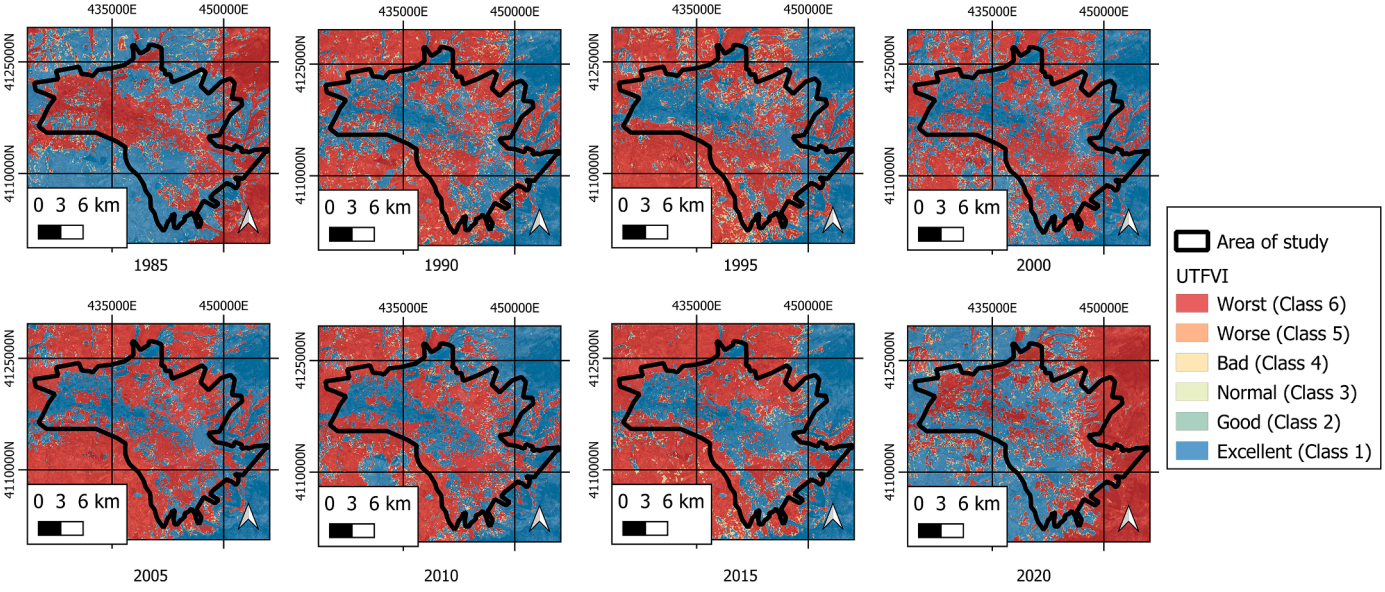

Fig. 12. UTFVI spatial pattern of the area studied, by years.

Table 5
Ecological evaluation of thermal comfort.

CLASS	UTFVI	UHI PRESENCE	ECOLOGICAL INDEX	1985 (%)	1990 (%)	1995 (%)	2000 (%)	2005 (%)	2010 (%)	2015 (%)	2020 (%)	Change (%)
1	< 0	NONE	EXCELLENT	45.9	44.0	43.3	42.8	39.3	42.1	37.4	34.5	**-25.5**
2	0 - 0.005	WEAK	GOOD	0.3	0.0	0.0	0.0	0.0	0.0	2.4	0.3	**-17.3**
3	0.005 - 0.010	MIDDLE	NORMAL	4.8	6.0	5.8	11.8	10.2	0.0	2.4	2.9	**-40.5**
4	0.010 - 0.015	STRONG	BAD	0.4	0.0	0.0	0.0	0.0	6.3	2.3	2.9	**62.4**
5	0.015 - 0.020	STRONGER	WORSE	4.9	5.8	6.0	0.0	0.0	0.0	2.3	5.3	**6.4**
6	> 0.020	STRONGEST	WORST	38.5	38.9	39.6	40.1	45.1	46.2	47.9	48.9	**26.2**

Table 6
Pearson's correlation coefficient for LST, NDVI, NDBI, PV, UI and LULC indices.

	LST	NDVI	PV	NDBI	UI	LULC
LST	1.000					
NDVI	-0.789	1.000				
PV	-0.539	0.743	1.000			
NDBI	0.812	-0.811	-0.638	1.000		
UI	0.654	-0.880	-0.659	0.970	1.000	
LULC	0.678	-0.158	-0.234	0.159	0.126	1.000

Table 7
LST results and NDVI, NDBI, PV, UI and LULC indices.

	β	ρ	sd
NDVI	-10.030	*0.000****	2.4137
PV	-15.805	*0.000****	3.6172
NDBI	5.2136	*0.006***	2.3461
UI	6.4142	*0.002***	2.0835
LULC	0.45713	*0.000****	0.0499
	R^2=0.79	F= 1286	Prob>chi^2= 0.000

β: Coefficient; sd: Standard deviation; Robust standard errors: *p<0.05, **p<0.01 and ***p<0.001.
R^2: Linear regression coefficient. F: Statistical.

Table 8
Pearson's correlation coefficient for LST and SUHI indices.

	LST	SUHI
LST	1.000	
SUHI	0.818	1.000

Table 9
LST and SUHI results.

	β	ρ	sd
SUHI	3.227	*0.000****	0.1034
	R^2=0.67	F= 973	Prob>chi^2= 0.000

β: Coefficient; sd: Standard deviation; Robust standard errors: *p<0.05, **p<0.01 and ***p<0.001.
R^2: Linear regression coefficient. F: Statistical.

Table 10
Pearson correlation coefficient for UHS, LST, SUHI and LULC indices.

	UHS	LST	SUHI	LULC
UHS	1.000			
LST	0.859	1.000		
SUHI	0.672	0.818	1.000	
LULC	0.195	0.678	0.238	1.000

Table 11
UHS results with LST, SUHI and LULC.

	β	ρ	sd
LST	0.0353	*0.000****	0.0101
SUHI	0.1172	*0.000****	0.0327
LULC	0.0210	*0.016**	0.0087
	R^2=0.55	F= 12.85	Prob>chi^2= 0.003

β: Coefficient; sd: Standard deviation; Robust standard errors: *p<0.05, **p<0.01 and ***p<0.001.
R^2: Linear regression coefficient. F: Statistical.

In the studied area, a drop is detected in the mean values of NDVI and PV, although high values are reported in rural areas with vegetation, in contrast to the lowest values found in urban areas. But there has been an increase in the mean values of the NDBI and UI indices, which remain high in urban areas as opposed to rural areas having vegetation, where the lowest values are located. From the LULC results, a significant decrease in water bodies, vegetation and farmland coverage is identified, while an increase in built-up and bare soil coverage is reported. The increases in the NDBI, UI and built-up land cover indexes reflect rapid urbanization of the studied area, caused by a conversion of land formerly used for agriculture or having vegetation. Such findings are in line with recent results (Amindin et al., 2021; Luo & Wu, 2021; Sharma et al., 2021) regarding other cities or territories. Studies on Iran (Amindin et al., 2021) reported 30% reductions in green space between 1995 and 2016, along with 30% increases in bare soil cover. In our research, the reduction of green areas is lower (10.8%), given that such areas in Spain are regarded as shields of protection against climate change. Notwithstanding, our results in terms of increased coverage of bare soil largely coincide, perhaps reflecting a trend of abandonment of farmland and agricultural practices *per se* since the 19th century in areas of the Mediterranean basin (Benayas et al., 2007). The agricultural crisis that Spain suffered at the beginning of the 20th century —in a context of economic development, high production costs, progressive industrialization, but also droughts and speculation, obeying a trend to transform these types of soils into urban ones and obtain a high profit— are common circumstances behind such increases in this type of coverage (Romero & Martínez, 2014). On the other hand, it is necessary to stress that the general decrease in NDVI and PV cannot be attributed only to a rise in built-up zones and a decrease in vegetation zones; it also attests to a progressive decrease in rainfall as a consequence of climate change (Li et al., 2002; Nicholson & Farrar, 1994). Indeed, according to AEMET data, 17 of the last 32 years have been classified as very dry in Spain.

The period 1985-2020 witnessed a considerable increase in LST and SUHI in the area studied. Such increments can be attributed to the building boom undergone in Granada (and elsewhere in Spain), to the detriment of green areas with vegetation. Authors Kotharkar and Surawar (2016) likewise evidenced this problem, concluding that a decrease in green areas means an increase in LST and SUHI, and vice versa. It has been shown that the greatest increases in LST and SUHI occur in areas with the lowest values in the NDVI and PV indices, and in

turn coincide with areas having the highest NDBI and UI values. These indicative relationships are supported by statistical analysis, giving strong negative correlations with the first indices and positive ones with the second. The highest correlation of the LST is that produced with the NDBI variable; the lowest is that obtained with PV. Evidence from previous studies would underline this close relationship between LST and NDBI compared to the rest, since it is completely independent of any possible modifications produced by climate change (Shahfahad et al., 2021; Tepanosyan et al., 2021). The use of waterproof construction materials with high thermal absorption in urban areas makes them give off the heat absorbed during the day, thereby raising the LST. The resulting increase in LST within urban areas implies greater differences with the LST of rural areas, thus contributing to the SUHI phenomenon (Saaroni et al., 2018; Singh et al., 2017; Wu et al., 2019; Yang et al., 2020). These reported relationships and circumstances, in line with the results obtained in other similar investigations (Ahmed, 2018; Guha et al., 2018; Luo & Wu, 2021; Sharma et al., 2021), serve to validate the results presented here. Still, it is important to remark that studies on certain areas of India (Sharma et al., 2021) and Iran (Amindin et al., 2021) show greater increases in LST (°C) than the area under study. This circumstance can be attributed to differences in population and surface between the studied areas, the one presented here (Granada) being smaller and less populated.

A significant increase in the areas classified as UHS is evidenced over our comparatively long study period. This circumstance would be motivated by: increased LST and SUHI, and decreasing vegetation zones in the area. Strong positive correlations between these variables are evidenced, reducing the UHS relationship with the LULC variable to weak, because the increases in UHS do not occur in all LULC covers, but mainly in those of the built-up and bare soil types. In our study, urban green areas with scarce vegetation, industrial areas, sports areas, roads and rural areas without vegetation are those giving the highest LST and SUHI values, thus contributing to a greater extent to the development of UHS. Numerous studies confirm that during early morning hours, solar radiation in areas of little vegetation or rural areas is greater than the radiation in urban areas. Shade generated by buildings and trees impedes the heating of enclosures and impermeable surfaces, and contributes to the cooling rates of vegetated areas (Li & Meng, 2018; Yang et al., 2020). Yet some studies involving satellite images show that vegetation has a cooling effect in urban areas (Lin et al., 2015; Tan et al., 2017; Yu et al., 2017) as well as a warming effect in areas with scarce vegetation and/or bare soils (Estoque et al., 2017; Lin et al., 2015). It is important to account for the processes of shading and evapotranspiration, as well as rates of cooling or heating by convection and transpiration. Such processes, by altering the LST of an urban area, would explain the behavior observed for the SUHI in this research. Numerous studies (Das et al., 2021; Guha et al., 2018; Jafari et al., 2021; Karimi et al., 2021; Shahfahad et al., 2021; Sharma et al., 2021) underline the significance of these factors, reporting results very similar to our findings.

Finally, significant deterioration of the general thermal comfort (UTFVI) within the area under study has been evidenced and can be interpreted as an alarm signal. Local areas associated with better comfort (classes 1, 2 and 3) and lower temperatures are being lost, just as worse areas (classes 4, 5 and 6) with higher temperatures increase considerably. In 2020, category 6 of the UTFVI developed mainly on built-up or bare soils, those usually giving higher temperatures. A number of studies conducted elsewhere (Guha, 2017; Kafy et al., 2021; Luo & Wu, 2021; Majumder et al., 2021; Shahfahad et al., 2021; Vimayak et al., 2022) corroborate significant increases in classes 4, 5 and 6 in urban areas, motivated by intense development and reflected by the LST, supporting the results presented here. Research carried out in India (Sharma et al., 2021) between 2011 and 2019 furthermore presents similar results (33.56%) in conjunction with a growth of category 6 (26.20%).

Conclusions

In recent years, the study of the UHS in conjunction with the environmental comfort index has become a field of analysis of great importance. Climate events point to a dire need to know which factors alter urban microclimates, so that we might establish mitigation measures in the framework of future urban proposals to sustain environmental comfort and ultimately improve the quality of life of citizens.

The present study describes the evolution of the LULC, LST and SUHI over 35 years (from 1985 to 2020) in the metropolitan area of Granada, southern Spain. Our aim was to evaluate how these indices, along with UI, NDVI, NDBI and PV, have influenced the increased UHS and the deterioration of the UTFVI.

The study area, during the period specified, underwent increases in the mean values of the NDBI and UI indices, while also showing reductions in the mean values of NDVI and PV. The LULC reflects substantial increases in built-up and bare soil coverage, accompanied by decreases in water bodies, vegetation and farmland coverage. This comes to confirm that the area under study has undergone rapid urban growth through the transformation of natural and agricultural land into urbanized or bare soil. The associated abandonment of farmland (owing to high production costs, droughts, progressive industrialization and land speculation by developers) is a very common trend in the arable lands of the Mediterranean basin. At the same time, there is ample evidence of a progressive rise in the LST and SUHI, especially since 2005, which has led to an increase in areas classified as UHS and a clear deterioration in the thermal comfort of the area assessed by means of the UTFVI index.

It is evident that the transformation of natural and agricultural land into urbanized or bare soil during the time interval studied is a main reason behind this increase in LST and SUHI, hence the ensuing increase in UHS zones and deterioration of UTFVI. The urban green areas having little vegetation, industrial areas, sports areas, roads and rural areas without vegetation in our study area show the greatest increases in LST and SUHI, contributing to a greater extent to the development of large UHS areas. Continued study and enhanced knowledge of these areas, backed by public administrations and urban planners, is essential to implement actions to correct such detrimental situations and establish measures to promote resilient future urban development.

Thus, these results urge us to underline the need for significant efforts to modify the upward trend of LST, SUHI, UHS and UTFVI values. One of the most effective strategies is to increase green spaces with vegetation, increasing the PV and NDVI indices. By fomenting vegetation cover that receives solar radiation but does not revert it to the atmosphere —as happens with impermeable materials and surfaces— a better thermal environment can be secured. This measure, if applied to vast surfaces, will eventually improve the quality of life of local inhabitants.

Our findings provide for a better understanding of the interaction that occurs between the LST, SUHI, UHS and UTFVI, as well as how they may be conditioned by the NDVI, NDBI, UI, PV and LULC indices. Hopefully, in the wake of research efforts such as this one, administrations in charge of future developmental plans can adopt appropriate mitigation and resilience measures to minimize or eliminate increases in LST and SUHI, which would quite clearly translate as a decrease in UHS and an improvement in UTFVI.

Study limitations

Concerning limitations to the study carried out, it is deemed necessary that future research endeavors should increase the number of years (or at least months) of analysis. This research contemplates just three images per year, and always in April. It would be wise for new studies to explore towns near Granada to verify if further variables or circumstances might be linked to research results. (Eqn. 5, 11-12).

Declaration of Competing Interest

The authors declare that they have no known competing financial interests or personal relationships that could have appeared to influence the work reported in this paper.

References

Ahmed, S. (2018). Assessment of urban heat islands and impact of climate change on socioeconomic over Suez Governorate using remote sensing and GIS techniques. *Egyptian Journal of Remote Sensing and Space Science, 21*(1), 15–25. https://doi.org/10.1016/j.ejrs.2017.08.001

Alcock, I., White, M. P., Lovell, R., Higgins, S. L., Osborne, N. J., Husk, K., & Wheeler, B. W. (2015). What accounts for "England's green and pleasant land"? A panel data analysis of mental health and land cover types in rural England. *Landscape and Urban Planning, 142*, 38–46. https://doi.org/10.1016/j.landurbplan.2015.05.008

Amindin, A., Pouyan, S., Pourghasemi, H. R., Yousefi, S., & Tiefenbacher, J. P. (2021). Spatial and temporal analysis of urban heat island using Landsat satellite images. *Environmental Science and Pollution Research, 28*(30), 41439–41450. https://doi.org/10.1007/s11356-021-13693-0

Anjos, M., Créso, A., Krecl, P., Yoshikazu, G., & Favaro, R. (2020). Analysisi of the urban heat island under different synoptic patterns using local climate zones. *Building and Environment, 185*, Article 107268. https://doi.org/10.1016/j.buildenv.2020.107268

Arbuthnott, K. G., & Hajat, S. (2017). The health effects of hotter summers and heat waves in the population of the United Kingdom: A review of the evidence. *Environmental Health: A Global Access Science Source, 16*(Suppl 1), 1–13. https://doi.org/10.1186/s12940-017-0322-5

Arnfield, A. J. (2003). Two decades of urban climate research: A review of turbulence, exchanges of energy and water, and the urban heat island. *International Journal of Climatology, 23*(1), 1–26. https://doi.org/10.1002/joc.859

Barbieri, T., Despini, F., & Teggi, S. (2018). A multi-temporal analyses of Land Surface Temperature using Landsat-8 data and open source software: The case study of Modena, Italy. *Sustainability (Switzerland), 10*, 1678. https://doi.org/10.3390/su10051678

Benayas, J. M. R., Martins, A., Nicolau, J. M., & Schulz, J. J. (2007). Abandonment of agricultural land: An overview of drivers and consequences. *CAB Reviews: Perspectives in Agriculture, Veterinary Science, Nutrition and Natural Resources, 2*(057). https://doi.org/10.1079/PAVSNNR20072057

Campbell, J. (1996). *Introduction to Remote Sensing* (2nd ed.). Taylor and Francis.

Čeplová, N., Kalusová, V., & Lososová, Z. (2017). Effects of settlement size, urban heat island and habitat type on urban plant biodiversity. *Landscape and Urban Planning, 159*, 15–22. https://doi.org/10.1016/j.landurbplan.2016.11.004

Chavez, P. S. (1988). An improved dark-object subtraction technique for atmospheric scattering correction of multispectral data. *Remote Sensing of Environment, 24*(3), 459–479. https://doi.org/10.1016/0034-4257(88)90019-3

Chen, Y., Li, X., Zheng, Y., Guan, Y., & Liu, X. (2011). Estimating the relationship between urban forms and energy consumption: A case study in the Pearl River Delta, 2005-2008. *Landscape and Urban Planning, 102*(1), 33–42. https://doi.org/10.1016/j.landurbplan.2011.03.007

Congedo, L. (2016). Semi-Automatic Classification Plugin Documentation Release 4.8.0.1. *Release, 4*(0.1), 29. https://doi.org/10.13140/RG.2.2.29474.02242/1

Das, A., Ghosh, S., Das, K., Basu, T., Dutta, I., & Das, M. (2021). Living environment matters: Unravelling the spatial clustering of covid-19 hotspots in Kolkata megacity, India. *Sustainable cities and society, 65*, Article 102577. https://doi.org/10.1016/j.scs.2021.102577

Das, M., & Das, A. (2020). Assessing the relationship between local climatic zones (LCZs) and land surface temperature (LST) – A case study of Sriniketan-Santiniketan Planning Area (SSPA), West Bengal, India. *Urban Climate, 32*, Article 100591. https://doi.org/10.1016/j.uclim.2020.100591. April 2019.

de Castro, M., Gallardo, C., Jylha, K., & Tuomenvirta, H. (2007). The use of a climate-type classification for assessing climate change effects in Europe from an ensemble of nine regional climate models. *Climatic Change, 81*(S1), 329–341. https://doi.org/10.1007/s10584-006-9224-1

Dwivedi, A., & Mohan, B. K. (2018). Impact of green roof on micro climate to reduce Urban Heat Island. *Remote Sensing Applications: Society and Environment, 10*, 56–69. https://doi.org/10.1016/j.rsase.2018.01.003

Emmanuel, R., & Krüger, E. (2012). Urban heat island and its impact climate change resilience in a shrinking city: The case of Glasgow, UK. *Building and Environment, 53*, 137–149. https://doi.org/10.1016/j.buildenv.2012.01.020

Estoque, R. C., Murayama, Y., & Myint, S. W. (2017). Effects of landscape composition and pattern on land surface temperature: An urban heat island study in the megacities of Southeast Asia. *Science of the Total Environment, 577*, 349–359. https://doi.org/10.1016/j.scitotenv.2016.10.195

Fang, L., & Tian, C. (2020). Construction land quotas as a tool for managing urban expansion. *Landscape and Urban Planning, 195*, Article 103727. https://doi.org/10.1016/j.landurbplan.2019.103727. May 2019.

Feizizadeh, B., & Blaschke, T. (2013). Examining Urban heat Island relations to land use and air pollution: Multiple endmember spectral mixture analysis for thermal remote sensing. *IEEE Journal of Selected Topics in Applied Earth Observations and Remote Sensing, 6*(3), 1749–1756. https://doi.org/10.1109/JSTARS.2013.2263425

Guha, S. (2017). Dynamic analysis and ecological evaluation of urban heat islands in Raipur city, India. *Journal of Applied Remote Sensing, 11*(03), 1. https://doi.org/10.1117/1.jrs.11.036020

Guha, S., Govil, H., Dey, A., & Gill, N. (2018). Analytical study of land surface temperature with NDVI and NDBI using Landsat 8 OLI and TIRS data in Florence and Naples city, Italy. *European Journal of Remote Sensing, 51*(1), 667–678. https://doi.org/10.1080/22797254.2018.1474494

Hidalgo, D., & Arco, J. (2021). Modeling of the Urban Heat Island on local climatic zones of a city using Sentinel 3 images: Urban determining factors. *Urban Climate, 37*, Article 100840. https://doi.org/10.1016/j.uclim.2021.100840

Hua, L., Zhang, X., Nie, Q., Sun, F., & Tang, L. (2020). The impacts of the expansion of urban impervious surfaces on urban heat islands in a coastal city in China. *Sustainability (Switzerland), 12*(2). https://doi.org/10.3390/su12020475

Jafari, A., Delikhoon, M., Rostoni, M., Baghani, A., Sorooshian, A., Rohani, M., Kermani, M., Rezai, R., Golbaz, S., & Golkhorshidi, F. (2021). Characteristics of gaseous and particulate air pollutants at four different urban hotspots in Tehran, Iran. *Sustainable cities and society, 70*, Article 102907. https://doi.org/10.1016/j.scs.2021.102907

Kafer, P. S., Rolim, S. B. A., Iglesias, M. L., Da Rocha, N. S., & Diaz, L. R. (2019). Land surface temperature retrieval by landsat 8 thermal band: Applications of laboratory and field measurements. *IEEE Journal of Selected Topics in Applied Earth Observations and Remote Sensing, 12*(7), 2332–2341. https://doi.org/10.1109/JSTARS.2019.2913822

Kafy, A. Al, Faisal, A. Al, Rahman, M. S., Islam, M., Rakib, Al, Islam, A., A, M., Khan, M. H. H., Sikdar, M. S., Sarker, M. H. S., Mawa, J., & Sattar, G. S. (2021). Prediction of seasonal urban thermal field variance index using machine learning algorithms in Cumilla, Bangladesh. *Sustainable Cities and Society, 64*, Article 102542. https://doi.org/10.1016/j.scs.2020.102542

Karakuş, C. B. (2019). The impact of land use/land cover (LULC) changes on land surface temperature in sivas city center and its surroundings and assessment of urban heat island. *Asia-Pacific Journal of Atmospheric Sciences, 55*(4), 669–684. https://doi.org/10.1007/s13143-019-00109-w

Karimi, N., Wai, K., & Richter, A. (2021). Prediction of fugitive landfill gas hotspots using a random forest algorithm and Sentinel 2 data. *Sustainable cities and society, 73*, Article 103097. https://doi.org/10.1016/j.scs.2021.103097

Kawamura, M., Jayamana, S., & Tsujiko, Y. (1996). Relation between social and environmental conditions in Colombo Sri Lanka and the urban index estimated by satellite remote sensing data. *International Archieve of Photogrammetry and Remote Sensing, 31*(B7), 321–326.

Khamchiangta, D., & Dhakal, S. (2019). Physical and non-physical factors driving urban heat island: Case of Bangkok Metropolitan Administration, Thailand. *Journal of Environmental Management, 248*, Article 109285. https://doi.org/10.1016/j.jenvman.2019.109285. July.

Kotharkar, R., & Surawar, M. (2016). Land use, Land Cover and population density impacto n the formation of canopy urban heat island through traverse survey in the Nagpur urban área, India. *Journal of Urban Planning and Development, 142*(1), Article 04015003. https://doi.org/10.1061/(ASCE)UP.1943-5444.000

Kovats, R. S., Campbell-Lendrum, D., & Matthies, F. (2005). Climate change and human health: Estimating avoidable deaths and disease. *Risk Analysis, 25*(6), 1409–1418. https://doi.org/10.1111/j.1539-6924.2005.00688.x

Labra, R. (2014). *Zero panel data guide*. Cátedra UA. file:///U:/Maguilera/Documentos-Personales-MAGUILERA/Master-M3F/Trabajo-Fin-M3F/Revisión-para-paper/Referencias/Stata/16_Guia-CERO-para-datos-de-panel_Un-enfoque-practico.pdf.

Li, B., Tao, S., & Dawson, R. W. (2002). Relations between AVHRR NDVI and ecoclimatic parameters in China. *International Journal of Remote Sensing, 23*(5), 989–999. https://doi.org/10.1080/014311602753474192

Li, J., Song, C., Cao, L., Zhu, F., Meng, X., & Wu, J. (2011). Impacts of landscape structure on surface urban heat islands: A case study of Shanghai, China. *Remote Sensing of Environment, 115*(12), 3249–3263. https://doi.org/10.1016/j.rse.2011.07.008

Li, T., & Meng, Q. (2018). A mixture emissivity analysis method for urban land surface temperature retrieval from Landsat 8 data. *Landscape and Urban Planning, 179*, 63–71. https://doi.org/10.1016/j.landurbplan.2018.07.010. July.

Li, X., Fan, W., Wang, L., Luo, M., Yao, R., Wang, S., & Wang, L. (2021). Effect of urban expansion on atmospheric humidity in Beijing-Tianjin-Hebei urban agglomeration. *Science of total environment, 759*, Article 144305. https://doi.org/10.1016/j.scitotenv.2020.144305

Lin, W., Yu, T., Chang, X., Wu, W., & Zhang, Y. (2015). Calculating cooling extents of green parks using remote sensing: Method and test. *Landscape and Urban Planning, 134*, 66–75. https://doi.org/10.1016/j.landurbplan.2014.10.012

Liu, L., & Zhang, Y. (2011). Urban heat island analysis using the landsat TM data and ASTER Data: A case study in Hong Kong. *Remote Sensing, 3*(7), 1535–1552. https://doi.org/10.3390/rs3071535

Luo, H., & Wu, J. (2021). Effects of urban growth on the land surface temperature: A case study in Taiyuan, China. *Environment, Development and Sustainability, 23*(7), 10787–10813. https://doi.org/10.1007/s10668-020-01087-0

Macintyre, H. L., Heaviside, C., Taylor, J., Picetti, R., Symonds, P., Cai, X. M., & Vardoulakis, S. (2018). Assessing urban population vulnerability and environmental risks across an urban area during heatwaves – Implications for health protection. *Science of the Total Environment, 610–611*, 678–690. https://doi.org/10.1016/j.scitotenv.2017.08.062

Majumder, A., Setia, R., Kingra, P. K., Sembhi, H., Singh, S. P., & Pateriya, B. (2021). Estimation of land surface temperature using different retrieval methods for studying the spatiotemporal variations of surface urban heat and cold islands in Indian Punjab. *Environment, Development and Sustainability, 23*(11), 15921–15942. https://doi.org/10.1007/s10668-021-01321-3

Meteorology Statal Agency (MSA). (2021). *Atlas of solar radiation in Spain*. Available from http://www.aemet.es/es/serviciosclimaticos/datosclimatologicos/atlas_radiacion_solar.

Mukherjee, F., & Singh, D. (2020). Assessing Land Use–Land Cover Change and Its Impact on Land Surface Temperature Using LANDSAT Data: A Comparison of Two Urban Areas in India. *Earth Systems and Environment, 4*(2), 385–407. https://doi.org/10.1007/s41748-020-00155-9

Nicholson, S. E., & Farrar, T. J. (1994). The influence of soil type on the relationships between NDVI, rainfall, and soil moisture in semiarid Botswana. I. NDVI response to rainfall. *Remote Sensing of Environment, 50*(2), 107–120. https://doi.org/10.1016/0034-4257(94)90038-8

Oke, T. R. (1987). *Boundary layer climates.* Routledge.

Otukei, J. R., & Blaschke, T. (2010). Land cover change assessment using decision trees, support vector machines and maximum likelihood classification algorithms. *International Journal of Applied Earth Observation and Geoinformation, 12*(SUPPL. 1). https://doi.org/10.1016/j.jag.2009.11.002

Rajeshwari, A. (2014). Estimation of land surface temperature of Dindigul district using landsat 8 data. *International Journal of Research in Engineering and Technology, 03*(05), 122–126. https://doi.org/10.15623/ijret.2014.0305025

Romero, A., & Martínez, C. (2014). Usos del suelo y abandono de tierras de cultivo en el Altiplano Jumilla-Yecla (Región de Murcia). *Geoecología, Cambio Ambiental y Paisaje: Homenaje Al Profesor José María García Ruiz, 479*. https://doi.org/10.21138/bage.2272

Rozenstein, O., Qin, Z., Derimian, Y., & Karnieli, A. (2014). Derivation of land surface temperature for landsat-8 TIRS using a split window algorithm. *Sensors (Switzerland), 14*(4), 5768–5780. https://doi.org/10.3390/s140405768

Rozos, E., Makropoulos, C., & Maksimović, Č. (2013). Rethinking urban areas: An example of an integrated blue-green approach. *Water Science and Technology: Water Supply, 13*(6), 1534–1542. https://doi.org/10.2166/ws.2013.140

Saaroni, H., Amorim, J. H., Hiemstra, J. A., & Pearlmutter, D. (2018). Urban Green Infrastructure as a tool for urban heat mitigation: Survey of research methodologies and findings across different climatic regions. *Urban Climate, 24*, 94–110. https://doi.org/10.1016/j.uclim.2018.02.001. October 2017.

Santamouris, M. (2020). Recent progress on urban overheating and heat island research. Integrated assessment of the energy, environmental, vulnerability and health impact. Synergies with the global climate change. *Energy and Buildings, 207*. https://doi.org/10.1016/j.enbuild.2019.109482

Sarrat, C., Lemonsu, A., Masson, V., & Guedalia, D. (2006). Impact of urban heat island on regional atmospheric pollution. *Atmospheric Environment, 40*(10), 1743–1758. https://doi.org/10.1016/j.atmosenv.2005.11.037

Schneider, A., Friedl, M. A., & Potere, D. (2010). Mapping global urban areas using MODIS 500-m data: New methods and datasets based on "urban ecoregions.". *Remote Sensing of Environment, 114*(8), 1733–1746. https://doi.org/10.1016/j.rse.2010.03.003

Scolozzi, R., & Geneletti, D. (2012). A multi-scale qualitative approach to assess the impact of urbanization on natural habitats and their connectivity. *Environmental Impact Assessment Review, 36*, 9–22. https://doi.org/10.1016/j.eiar.2012.03.001

Seto, K. C., & Kaufmann, R. K. (2003). Modeling the drivers of urban land use change in the Pearl River Delta, China: Integrating remote sensing with socioeconomic data. *Land Economics, 79*(1), 106–121. https://doi.org/10.2307/3147108

Shafri, H. Z., & Ramle, F. S. (2009). A comparison of Support Vector Machine and Decision tree classifications using satellite data of Langkawi island. *Information Technology Journal, 8*(1), 64–70. https://doi.org/10.3923/itj.2009.64.70

Shahfahad, Talukdar, S., Rihan, M., Hang, H. T., Bhaskaran, S., & Rahman, A. (2021). Modelling urban heat island (UHI) and thermal field variation and their relationship with land use indices over Delhi and Mumbai metro cities. *Environment, Development and Sustainability*. , Article 0123456789. https://doi.org/10.1007/s10668-021-01587-7

Sharma, R., Pradhan, L., Kumari, M., & Bhattacharya, P. (2021). Assessing urban heat islands and thermal comfort in Noida City using geospatial technology. *Urban Climate, 35*, Article 100751. https://doi.org/10.1016/j.uclim.2020.100751. August 2020.

Singh, P., Kikan, N., & Verma, P. (2017). Impact of land use change and urbanization on urban heat island in Lucknow city, central India. A remote sensing based estimate. *Sustainable cities and society, 32*, 100–114. https://doi.org/10.1016/j.scs.2017.02.018

Sobrino, J. A., & Irakulis, I. (2020). A methodology for comparing the surface urban heat Island in selected urban agglomerations around the world from Sentinel-3 SLSTR data. *Remote Sensing, 12*(12), 1–31. https://doi.org/10.3390/RS12122052

Song, J., Chen, W., Zhang, J., Huang, K., Hou, B., & Prishchepov, A. V. (2020). Effects of building density on land surface temperature in China: Spatial patterns and determinants. *Landscape and Urban Planning, 198*, Article 103794. https://doi.org/10.1016/j.landurbplan.2020.103794. March.

Song, J., Lin, T., Li, X., & Prishchepov, A. V. (2018). Mapping urban functional zones by integrating very high spatial resolution remote sensing imagery and points of interest: A case study of Xiamen, China. *Remote Sensing, 10*(11). https://doi.org/10.3390/rs10111737

Statistics National Institute (SNI). (2021). *Official population figures resulting from the revision of the Municipal Register as of January 1*. Available from https://www.ine.es/jaxiT3/Tabla.htm?t=2871.

Tan, K., Liao, Z., Du, P., & Wu, L. (2017). Land surface temperature retrieval from Landsat 8 data and validation with geosensor network. *Frontiers of Earth Science, 11*(1), 20–34. https://doi.org/10.1007/s11707-016-0570-7

Tepanosyan, G., Muradyan, V., Hovsepyan, A., Pinigin, G., Medvedev, A., & Asmaryan, S. (2021). Studying spatial-temporal changes and relationship of land cover and surface Urban Heat Island derived through remote sensing in Yerevan, Armenia. *Building and Environment, 187*, Article 107390. https://doi.org/10.1016/j.buildenv.2020.107390. October 2020.

Tsou, J., Zhuang, J., Li, Y., & Zhang, Y. (2017). Urban heat island assessment using the landsat 8 data: A case study in Shenzhen and Hong Kong. *Urban Science, 1*(1), 10. https://doi.org/10.3390/urbansci1010010

UN. (2018). *68% of the world population projected to live in urban areas by 2050, says UN*. https://www.un.org/development/desa/en/news/population/2018-revision-of-world-urbanization-prospects.html.

Vimayak, B., Lee, H., Gedam, S., & Latha, R. (2022). Impacts of future urbanization on urban microclimate and thermal comfort over the Mumbai metropolitan region, India. *Sustainable cities and society, 79*, Article 103703. https://doi.org/10.1016/j.scs.2022.103703

Weng, Q., Lu, D., & Schubring, J. (2004). Estimation of land surface temperature-vegetation abundance relationship for urban heat island studies. *Remote Sensing of Environment, 89*(4), 467–483. https://doi.org/10.1016/j.rse.2003.11.005

Wu, C., Li, J., Wang, C., Song, C., Chen, Y., Finka, M., & La Rosa, D. (2019). Understanding the relationship between urban blue infrastructure and land surface temperature. *Science of the Total Environment, 694*. https://doi.org/10.1016/j.scitotenv.2019.133742

Xu, D., Kang, X., Qiu, D., Zhuang, D., & Pan, J. (2009). Quantitative assessment of desertification using Landsat data on a regional scale - a case study in the Ordos Plateau, China. *Sensors, 9*(3), 1738–1753. https://doi.org/10.3390/s90301738

Yang, C., Yan, F., & Zhang, S. (2020). Comparison of land surface and air temperatures for quantifying summer and winter urban heat island in a snow climate city. *Journal of Environmental Management, 265*, Article 110563. https://doi.org/10.1016/j.jenvman.2020.110563. March.

Yao, R., Wang, L., Huang, X., Gong, W., & Xia, X. (2019). Greening in rural areas increases the surface urban heat island intensity. *Geophycal Research Letters, 46*(4), 2204–2212. https://doi.org/10.1029/201861081816

Yao, R., Wang, L., Huang, X., Liu, Y., Niu, Z., Wang, Sh., & Wang, L. (2021). Long-term trends of surface and canopy laye urban heat island intensity in 272 cities in the mainland of China. *Science os Total Environment, 609*, 742–754. https://doi.org/10.1016/j.scitontenv.2017145607

Yoo, C., Han, D., Im, J., & Bechtel, B. (2019). Comparison between convolutional neural networks and random forest for local climate zone classification in mega urban areas using Landsat images. *ISPRS Journal of Photogrammetry and Remote Sensing, 157*, 155–170. https://doi.org/10.1016/j.isprsjprs.2019.09.009. February.

Yu, X., Guo, X., & Wu, Z. (2014). Land surface temperature retrieval from landsat 8 TIRS-comparison between radiative transfer equation-based method, split window algorithm and single channel method. *Remote Sensing, 6*(10), 9829–9852. https://doi.org/10.3390/rs6109829

Yu, Y., Liu, Y., Yu, P., Liu, Y., & Yu, P. (2017). Land surface temperature product development for JPSS and GOES-R missions. *Comprehensive Remote Sensing, 1–9*, 284–303. https://doi.org/10.1016/B978-0-12-409548-9.10522-6

Zha, Y., Gao, J., & Ni, S. (2003). Use of normalized difference built-up index in automatically mapping urban areas from TM imagery. *International Journal of Remote Sensing, 24*(3), 583–594. https://doi.org/10.1080/01431160304987

Zhang, Y., Chen, L., Wang, Y., Chen, L., Yao, F., Wu, P., Wang, B., Li, Y., Zhou, T., & Zhang, T. (2015). Research on the contribution of urban land surface moisture to the alleviation effect of urban land surface heat based on landsat 8 data. *Remote Sensing, 7*(8), 10737–10762. https://doi.org/10.3390/rs70810737